

A hybrid calibration scheme for developing hydrogen enrichment ratio control map using RSM and ANN technique to enhance the characteristics of an ammonia biodiesel RCCI combustion engine

R. Elumalai, K. Ravi *

School of Mechanical Engineering, VIT University, Vellore, India



ARTICLE INFO

Handling Editor: Huihe Qiu

Keywords:

Hydrogen enrichment energy share
Ammonia energy premixing
Algal biodiesel: RCCI combustion
RSM and ANN based hybrid calibration scheme

ABSTRACT

This investigation aims to optimally attune hydrogen enrichment ratio for an ammonia biodiesel powered RCCI engine using RSM and ANN techniques. Conventionally, optimal mapping is accomplished through trial-and-error experimentation. In this study, an innovative model-based calibration method for developing an optimal hydrogen ratio map is suggested. The LRF energy share of ammonia in premixing is set at 40%, the hydrogen enrichment is varied from 5 to 20%, and the rest of the energy is biodiesel as HRF. Based on the experimental inputs, the RSM-based optimization has established an ideal hydrogen enrichment ratio of 14.77%, 18.75%, 18.93%, 17.94%, 16.43%, 14.42%, 15.58%, 13.23%, and 17.12% for intermittent load conditions of 20%, 30%, 40%, 50%, 60%, 70%, 80%, 90%, and 100%. A simultaneous decrease in smoke and BSEC is obtained, with a little penalty in NO_x emissions at optimal conditions. RSM optimization with a desirability level of 97.9% was conducted over three trials for authentication using ANN. Based on the results, ANN predicts all the replies with $R > 0.96$. The experimental corroboration of the predicted variables of the optimized map for 50% load has an error between 1.40% and 4.95%, which are within the acceptable range.

1. Introduction

As the world economy expands, the problem of greenhouse gases and climate disruption becomes more important [1]. The most significant greenhouse gas is carbon dioxide (CO₂). From 2020, some countries have proposed carbon neutrality targets; therefore, areas that reduce CO₂ emissions will have significant growth [2]. The internal combustion engine is an effective heat conversion technology that is crucial to contemporary society. Nevertheless, the controversy surrounding CO₂ and the polluting emissions of Compression Ignition (CI) engines powered by fossil fuels has focalized on the development of alternative fuels [3,4]. As can be seen, extensively depending on fossil fuels is not a sustainable approach, and the general tendency is to investigate the potential applications of carbon-free fuels [5]. The two carbon-free fuels that garnered the greatest interest recently are ammonia and hydrogen [6]. Because combustion of hydrogen/ammonia doesn't result in carbon emissions [5,7].

1.1. Biodiesel as IC engine fuel

Diesel engines are most prominent, because of their exceptional endurance and strong design [8–11]. Nonetheless, there has always been concern about the engine out emissions of diesel engines [12]. CI engines produce a substantial amount of smoke and NO_x

* Corresponding author.

E-mail addresses: ravi.krishnaiah@vit.ac.in, ravikrish97@gmail.com (K. Ravi).

emissions [13,14]. The chemical energy of fuel is used by the CI engine to produce mechanical work. During the combustion of diesel fuel, CO, NO_x, HC, and smoke are all produced [15]. One appealing alternative to diesel engines would be biodiesel [16–18]. Due to its lack of production and commercialization, biodiesel faces considerable obstacles [19,20]. Biodiesel production from first-generation edible feedstocks such as soybean, canola, mustard, palm, peanut, sunflower, and rapeseed had a negative influence on the human-food chain during production but was blamed for the skyrocketing costs of edible oil [21–24]. Supply chain constraints and a shortage of cultivable land have stymied the development of second-generation biodiesel, which employed non-edible feedstocks including mahua, kusum, and rubber seed [25–27]. Microalgae oil, a different kind of biodiesel made from algae, is used as a substitute for diesel since it has fuel properties similar to diesel [28]. Also, it was discovered that neat bio-oil causes poor oxidation stability, deposit development, and engine component corrosion [29,30]. Compared to diesel, biodiesel oil has a greater viscosity because of its chemical structure and molecular mass. This represents a significant impediment to the use of microalgae oil in diesel engines [31,32]. The viscosity of microalgae oil, atomization of fuel, and spray characteristics are all greatly impacted by the fuel droplet size, which decreases performance and raises harmful gas emissions [33]. Transesterification is one of the most frequently used chemical pre-treatment techniques in the world, and microalgae methyl ester could be used in a diesel engine without any hardware modification to reduce the viscosity of microalgae oil [34,35].

1.2. Ammonia as IC engine fuel

An investigation reported that, the only fuel for internal combustion engines that will meet the 2050 energy transition objective would be ammonia or an ammonia-hydrogen blend [36]. Ammonia provides numerous advantages as an alternate fuel, including the absence of pollutants, the cheapest cost of storage, ease of manufacture, better heating value, and energy conservation [37,38]. Foremost, ammonia burning doesn't emit carbon emissions, which meet current international standards [39]. Moreover, ammonia is readily soluble in water; it does not escape or leak and become another pollutant [40]. Compared to liquid hydrogen, ammonia can be transported and stored in comparatively moderate circumstances (240K at ambient temperature and pressure of around 10 bar) [41]. While liquid ammonia has a heating value that is manifestly larger than that of liquefied hydrogen, its storage cost is around half that of liquefied hydrogen [42]. The lowest temperature at which ammonia will ignite in air is higher than the lowest temperature at which Hydrogen (H₂) and hydrocarbon fuels will ignite, and the likelihood that ammonia fuel will ignite if it accidentally leaks during use or storage, is much lower propensity. Also, we can rapidly take the necessary steps to prevent an accident by smelling when ammonia seeps [43]. Therefore, ammonia has steadily gained attention as a prospective CI engine fuel and has the potential to become a widespread fuel in the future [44]. The potential of ammonia as a fuel for CI engines has received attention because of its characteristics, and several experiments have been conducted on ammonia fuel.

1.3. Reactivity controlled Compression Ignition

Ammonia is ideal for CI engines with high compression ratios because of its high-octane number (130), which does not guarantee a decreased knock propensity [45]. Ammonia has a high energy potential and liquefies. Ammonia has many drawbacks for engine applications, including a high auto-ignition temperature, sluggish turbulent flame speed, and narrow flammability, making it difficult to utilize as a sole fuel in CI engines [46,47]. The dual-fuel RCCI combustion approach has been shown to be a viable and promising method of using low-reactivity fuels such as gasoline, natural gas, hydrogen, and methanol in CI engines while improving thermal efficiency and lowering pollutants [48–50]. This technology aims to remove the technical barriers of CI engines. As a result, it is also anticipated that dual fuel combustion would increase the availability of ammonia in CI engines. Nevertheless, dual fuel combustion techniques that combine an ammonia premixed charge with a direct injection of high-reactivity fuel, such as biodiesel, diesel, have the potential to lower the engine out emissions [51].

1.4. Hydrogen as IC engine fuel

Researchers are focusing on resolving the aforementioned difficulties in ammonia combustion, which may be convalescent from hydrogen's excellent properties. In addition to employing alternative fuels such as hydrogen, ammonia fuels offer substantial benefits over fossil fuels because of their clean combustion, which is under consideration for use in CI engines [52]. Because of its high auto-ignition temperatures, hydrogen is difficult to employ in CI engines, necessitating a very high compression ratio [53]. It may be combined with fuels with lower auto-ignition temperatures [54,55]. Gaseous hydrogen is a good blending ingredient and may be used effectively due to its low ignition temperature and high flammability [56,57]. Hydrogen is distinguished from other gases by its high calorific value, short quenching distance, flame velocity, flammability limit, and diffusivity [58]. The enhancement in performance and pollutants such as CO, HC, and smoke are decreased in dual-fuel mode hydrogen operation [59]. Liew et al. [60] explored the diesel engine utilizing H₂ as the principal fuel at various load conditions and discovered that increasing the hydrogen share increased the peak HRR and maximum cylinder pressure. Cinivin and Kose [61] evaluated the effect of hydrogen share at full load conditions and found an increasing trend of thermal efficiency with reduced BSEC. In addition to that, exhaust pollutants such as CO, HC, and smoke were reduced while increasing NO_x emissions.

1.5. Optimization and prediction

Considering all the engine characteristics, evaluating a new fuel as an alternative to fossil fuels may require many tests. When both cost and time are considered, an inefficient scenario occurs. Several software applications have been implemented to improve the efficiency of the fuel map development process. With many of these computer applications, numerous simulations were performed with excellent precision, limiting the number of tests. Taguchi is one of these applications that determines the optimal amounts of all the variables and indicates which of the specified input variables are the most effective. RSM and ANN are mathematical approaches

that were often used to evaluate the effect of each input variable on the output variable, particularly when the output response was impacted by more than three independent variables. By using a hybrid approach, the efficiency of the process may be increased by simultaneously using ANN model-based prediction and RSM to identify the optimal combination of two or more input variables [62–65].

Experiments were developed in research utilizing Taguchi's L27 orthogonal array. Engine load, 2-ethylhexyl nitrate blend ratio, and biodiesel blend ratio were used as control factors. Optimization has been carried out to acquire the optimal combination of control factors for obtaining the response parameters. The error rate in the results varies from 0.87% to 9.42% compared with experimental results [66]. The main limitation of the Taguchi approach is that the findings are merely relative and do not specify which factor has the greatest influence on response value. A similar study was conducted using Response Surface Methodology (RSM), and the findings demonstrated that there is an excellent deal of agreement between the optimization and experiment results, and the error rate in the results varies from 0.63% to 4.57% compared with experimental values [67]. The RSM technique stands out among them because of its great accuracy and ease of use [68,69]. Unlike other optimization approaches, RSM determines statistically an experimental matrix with a minimum number of experiments and optimizes the factors and responses using the multi-objective optimization technique [70, 71]. Many researchers have chosen RSM to reduce the number of tests while optimizing engine factors and responses [72].

A study used ANN and RSM to identify the optimal blend of animal waste fat biodiesel. According to the RSM regression findings, all responses had absolute percentage of variance (R^2) values larger than 0.95. The ANN correlation coefficient (R) values were found to be greater than 0.97. Furthermore, based on the verification test between the optimal and predicted findings, it was determined that there is a good agreement with a maximum error rate of 3.863% [73]. For a more accurate forecast of CI combustion driven by biodiesel-mixed diesel fuel, Yusaf et al. [74] applied the ANN approach. The outcome demonstrates that, when compared to the RSM model, the constructed ANN model was more accurate in forecasting the replies. The motivation and novelty of this research were generally outlined in the following section, using literature as a foundation.

2. Motivation and objective

The use of ammonia in CI engines and hydrogen has appreciable effects on engine-out characteristics. In contrast, ammonia exhibits some deficiencies in combustion properties, so recommending ammonia as an alternative fuel to fossil fuels based on engine-out properties is inadequate. Therefore, it is necessary to evaluate the behaviors of hydrogen enhancement to overcome the deficiencies of ammonia combustion owing to its superior characteristics. Extensive research has been done to evaluate the impact of ammonia and biodiesel in CI engines. However, most of the research uses ammonia with common fuels like diesel, biodiesel, DEE, etc. in dual fuel mode. The intention of this investigation is to minimize the use of hydrocarbon fuels and improve carbon-free fuels. Furthermore, adding hydrogen to ammonia would improve combustion efficiency because of the superior characteristics of hydrogen.

To achieve the high standards of ammonia and biodiesel combustion efficiency in CI engines, a thorough analysis of the RCCI behaviors of ammonia, hydrogen, and biodiesel energy sharing for combustion, performance, and emission at diverse load conditions is essential. It is clear from the literature that ammonia's combustion properties when used with other fuels are being studied. Additionally, basic ammonia/biodiesel RCCI engines with hydrogen enrichment have not been studied in terms of balancing combustion, performance, and emission requirements. In order to fill this gap, the combustion, performance, and emission behaviors of ammonia, hydrogen, and biodiesel in RCCI engines were examined. The present study's goal is to focus on how different hydrogen fractions burn with ammonia or biodiesel in a dual-fuel RCCI engine. This kind of analysis would help to clarify how hydrogen, ammonia, and biodiesel are burned in RCCI engines and how the emissions are emitted. The data obtained could help improve how ammonia is used as fuel in CI engines. The use of numerical methods (RSM and ANN) to optimize the outcome and forecast the input parameters was another innovative aspect of this research. When these technologies are applied, the time and expense required for experimentation are considerably reduced, and the system's efficiency is improved. In order to create the best empirical model, the

Table 1
Properties of test fuels.

| Property | Microalgae biodiesel | Ammonia | Hydrogen |
|--|----------------------|---------|----------|
| Viscosity (cSt) at 40°C | 5.07 | — | — |
| Density (g/ml) at 20°C | 0.876 | 0.732 | 0.08 |
| Flame burning velocity (m/s) | 0.31 | 0.32 | 3.24 |
| Higher calorific value (MJ/kg) | 41.079 | 22.5 | 141.8 |
| Lower calorific value (MJ/kg) | 38.34 | 18.49 | 120 |
| Mass diffusivity in air (cm ² /s) | — | 0.22 | 0.61 |
| Latent heat of evaporation (kJ/kg) | 306 | 1371 | 461 |
| Cetane number | 42 | — | — |
| Octane number | — | 130 | 130 |
| Auto ignition temperature (°K) | 523 | 651 | 858 |
| Minimum ignition energy (mJ) | — | 8 | 0.02 |
| Flash point (°C) | 91 | 132 | — |
| Fir point (°C) | 121 | 148 | — |
| Boiling point (°C) | 340 | -33.34 | -252.9 |
| Freezing point (°C) | -30 | -77 | -259 |
| Flammability limit (% volume) | 0.6–7.5 | 14–33.8 | 4–75 |
| Stoichiometric A/F ratio | — | 6.06 | 34.36 |

Table 2
Experimental matrix.

| Operating mode | Energy Fraction | Mass flow rate (kg/h) | | | | | | | | | | | | Acronym | | | |
|----------------|-----------------|-----------------------|----------------|-------|-----------------|----------------|-------|-----------------|----------------|-------|-----------------|----------------|-------|---------|-------|-------|--------------------------|
| | | 20% Load | | | 40% Load | | | 60% Load | | | 80% Load | | | | | | |
| | | NH ₃ | H ₂ | BD | NH ₃ | H ₂ | BD | NH ₃ | H ₂ | BD | NH ₃ | H ₂ | BD | | | | |
| RCCI | 40/-/60 | 0.341 | 0 | 0.226 | 0.546 | 0 | 0.363 | 0.663 | 0 | 0.440 | 0.759 | 0 | 0.504 | 0.889 | 0 | 0.590 | 40%NH ₃ +0%H |
| | 40/05/55 | 0.334 | 0.005 | 0.203 | 0.530 | 0.009 | 0.322 | 0.636 | 0.010 | 0.387 | 0.721 | 0.012 | 0.439 | 0.836 | 0.014 | 0.509 | 40%NH ₃ +5%H |
| | 40/10/50 | 0.328 | 0.011 | 0.181 | 0.514 | 0.017 | 0.284 | 0.611 | 0.020 | 0.338 | 0.685 | 0.022 | 0.379 | 0.786 | 0.026 | 0.435 | 40%NH ₃ +10%H |
| | 40/15/45 | 0.321 | 0.016 | 0.160 | 0.498 | 0.024 | 0.248 | 0.586 | 0.029 | 0.292 | 0.651 | 0.032 | 0.324 | 0.739 | 0.036 | 0.368 | 40%NH ₃ +15%H |
| | 40/20/50 | 0.315 | 0.021 | 0.139 | 0.483 | 0.032 | 0.214 | 0.563 | 0.037 | 0.249 | 0.618 | 0.040 | 0.274 | 0.694 | 0.045 | 0.307 | 40%NH ₃ +20%H |

working function of RSM is a kind of statistically based inquiry that successfully establishes interaction between the many components. In the present study, RSM was used to create a regression model and find the optimal hydrogen premix percentage. In addition, an ANN model was developed to more accurately predict the response under different load conditions with hydrogen concentration.

3. Materials and methods

3.1. Energy fraction methodology

The tests included in the study's scope were carried out under various loads and at 1500 rpm. The energy shares of the hydrogen, ammonia, and biodiesel, which were determined using Equation (1), were detailed as the ratio of the respective energies of the ammonia, hydrogen, and biodiesel to the sum of the energies supplied to the combustion. Where m_{H_2} , m_{NH_3} , and m_{BD} are the mass flow rates of hydrogen, ammonia, and biodiesel fuels, respectively, CV_{H_2} , CV_{NH_3} , and CV_{BD} are the calorific values of hydrogen, ammonia, and biodiesel fuels. The investigation engine initially warmed to 80°C to establish stable conditions prior to starting the data collection operation. The tests were run three times in order to reduce the amount of error in the data acquired, and the assessments were conducted by averaging the results. The properties of fuels are displayed in Table 1.

$$\% \text{NH}_3 / \% \text{H}_2 / \% \text{Biodiesel} = \frac{(m_{\text{NH}_3} \times \text{CV}_{\text{NH}_3}) \text{ or } (m_{\text{H}_2} \times \text{CV}_{\text{H}_2}) \text{ or } (m_{\text{BD}} \times \text{CV}_{\text{BD}})}{(m_{\text{BD}} \times \text{CV}_{\text{BD}}) + (m_{\text{NH}_3} \times \text{CV}_{\text{NH}_3}) + (m_{\text{H}_2} \times \text{CV}_{\text{H}_2})} \times 100 \quad (1)$$

3.2. LRF supply system

Gaseous hydrogen is introduced into the cylinder intake manifold during suction. The gaseous hydrogen, maintained at 150 bar, is directed through a pressure regulator, a mass flow metre (model FT3), a flame arrester, and finally a flame trapper into the intake manifold. The injection of the gaseous fuel is started at 355°CA in the suction stroke, and the hydrogen induction valve is kept open throughout the injection stroke. A 150-lb ammonia cylinder was used to hold the liquid ammonia. The ammonia cylinder temperature was maintained at 38°C using a heater blanket attached to the ammonia cylinder and directed through a pressure regulator, a mass flowmeter (model FT3) for ammonia, and finally a solenoid injector into the intake manifold. Prior to ammonia injectors, a gas chamber was added to decrease flow pulsation caused by pressure changes. Vapor ammonia is being injected into the manifold using an electronically controlled PFI system. Pulse lengths, injector pressure, and timings were all regulated by the ECU. By varying the input voltage of the injector, the ammonia energy premixing fraction was achieved. In both cases, the pressure regulator lowers the massive input pressure to the required outlet pressure and regulates the flow of gases. Additionally, they strive to keep the outlet pressure constant despite variations in the intake pressure. The mass flow rate of gaseous hydrogen must be adjusted by passing a precision flow control valve before the hydrogen flowmeter. A flashback arrestor was utilized in the hydrogen induction system, which prohibited reverse hydrogen flow. A flame trapper was finally used before intake, therefore decreasing the possibility of flashback. Biodiesel fuel was injected using the conventional fuel injection system. The flow of biodiesel as pilot fuel was controlled by the

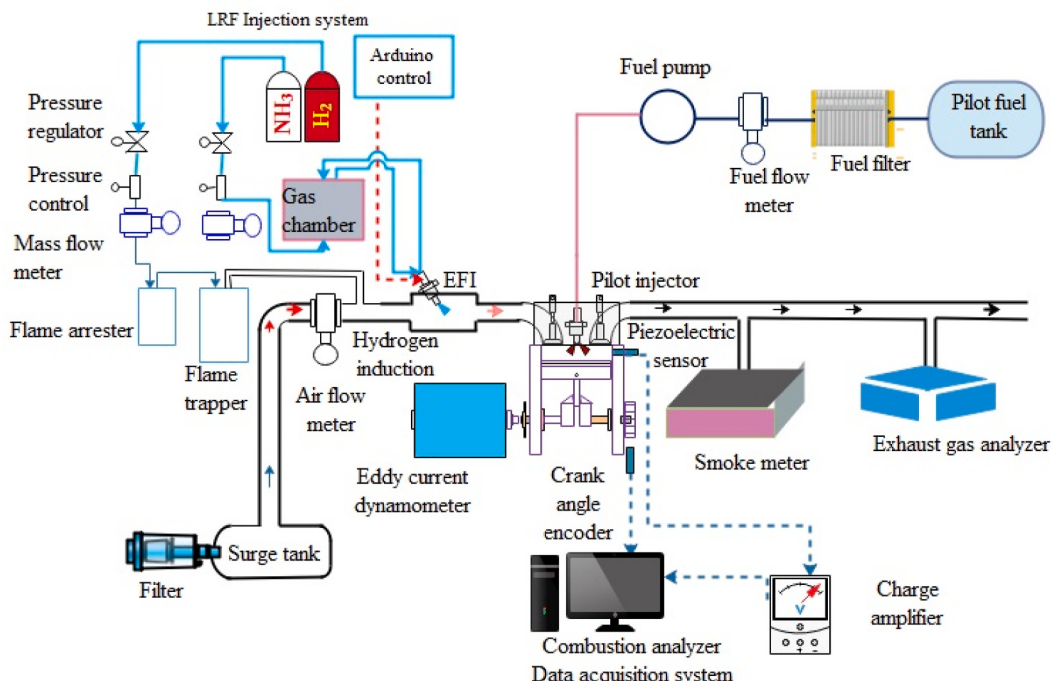


Fig. 1. Experimental setup.

governor.

3.3. Operating condition

This study has evaluated the characteristics of a CI engine running on biodiesel, hydrogen, and ammonia. The energy share of ammonia in premixing is set at 40%, the enrichment of hydrogen varies from 5 to 20%, and the rest of the energy is biodiesel at different loading conditions by maintaining a constant engine rpm of 1500. Table 2 represents the flow rates of the test fuels. Ammonia has a lower calorific value than biodiesel and hydrogen, requiring a larger mass flow rate to provide the same amount of power as pure biodiesel. As the hydrogen ratio rises, the mixture's stoichiometric air-to-fuel ratio increases since hydrogen has a higher stoichiometric air-to-fuel ratio [75]. Therefore, induction of hydrogen into the intake manifold was limited to 20% in this current study. Further adding hydrogen to the combustion leads to a reduction in the intake of oxygen.

3.4. Experimental setup

For conducting experimental research with various gaseous fuel mixes, a gaseous fuel mixing setup was developed, as shown in Fig. 1. It consists of a mono cylinder CI engine, an eddy-current dynamometer, and a hydrogen and ammonia fuel supply system. Other details about the engine setup are listed in Table 3. Table 4 contains the precise technical details of the engine configuration, together with the measurement uncertainty and instrument accuracy. The earlier study efforts were utilized as a reference for the ideal ammonia energy premixing. Gaseous fuel supply lines (such as those for ammonia and hydrogen) were established, and pressure regulators were used to limit pressures from storage cylinders. The gaseous hydrogen ammonia from the distribution line is routed to the relevant mass flow regulators, which regulate the flow with the necessary composition to the engine. An electronically injected ammonia fuel was directed to the gas chamber, which lessened the likelihood of pressure variations.

The quantity of gaseous fuel premix is regulated with the use of a pressure regulator and delivered into the engine's intake manifold, where it is mixed with air. The in-cylinder combustion pressure was recorded in the data collection system using piezoelectric pressure transducers (Kistler manufacture) with charge amplifiers. In order to achieve a valid response rate for research on combustion variables, the cylinder pressures were collected for 100 successive cycles. The directly injected biodiesel was controlled by the governor effect, while the manifold injection of gaseous ammonia was adjusted manually through an ECU, and hydrogen was manually inducted through the manifold. The flow rate of fuel was quantified in kg/s. The engine emissions were recorded by the gas analyzer. A K-type thermocouple and an optical crank-angle encoder (0.1CAD CAD resolution) are additional tools connected to the engine test bed.

3.5. Uncertainty

To evaluate the uncertainties of observed parameters with $+2\sigma$ confidence intervals, the Gaussian-distribution technique was utilized. Measurements were taken under identical operating circumstances to estimate uncertainty.

The uncertainty associated with the measured parameter is expressed as $(\Delta X_i) = 2 \sigma_i / \bar{X}_i * 100$

The root-mean-square technique is used to provide accurate error bounds for the calculated factors, and the degree of the error is represented by equation (2).

$$\Delta R = \sqrt{\left((\partial R / \partial X_1 * \Delta X_1)^2 + (\partial R / \partial X_2 * \Delta X_2)^2 + \dots + (\partial R / \partial X_n * \Delta X_n)^2 \right)} \quad (2)$$

The experiment overall percentage of uncertainty is:

$$= \sqrt{0.8^2 + 0.9^2 + 0.8^2 + 0.8^2 + 1.3^2 + 1.1^2 + 0.9^2 + 1.3^2} = 2.85\%$$

3.6. Response surface method

There are several input parameters for internal combustion engines. The costs and time for examining the interactions between these input parameters are relatively high. In such experimental research, the RSM procedure may be made more effective by reducing both the cost and the time involved. Numerical modelling is incorporated after acquiring the experimental set using the RSM approach. The experimental values generated by the constructed numerical model are the most precise means of determining the response

Table 3
Engine setup.

| Parameters | Particulars |
|--------------------------|---------------|
| Made | Kirloskar |
| Cooling type | Water cooling |
| Power output (kW) | 3.5 |
| Compression Ratio | 17.5 |
| SoI (direct injection) | 24°CA bTDC |
| Speed (rpm) | 1500 |
| Bore × stroke (mm) | 87.5 × 110 |
| Injection Pressure (bar) | 230 |
| Torque (N·m) | 23.5 |
| Dynamometer model | Eddy Current |

Table 4
Uncertainty analysis.

| Parameters | % Accuracy limit | % Uncertainty |
|--|------------------|---------------|
| Brake power (BP) (kW) | ±0.4 | ±0.8 |
| Fuel consumption (g/s) | ±0.62 | ±0.9 |
| Pressure (bar) | ±0.41 | ±0.8 |
| Hydrocarbon (HC) (ppm) | ±5.25 | ±0.8 |
| Speed (N) (rpm) | ±0.26 | ±1.3 |
| Smoke opacity (%) | ±1.33 | ±1.1 |
| Carbon monoxide (CO) (% vol) | ±0.08 | ±0.9 |
| Nitrogen oxides (NO _x) (ppm) | ±2.35 | ±1.3 |

parameter values, irrespective of the intermediate outcomes and boundary limits. Reducing the total number of RSM experiments also aids in identifying the ideal input variables, considering the desired response outcomes and the values attained via the use of experimental techniques.

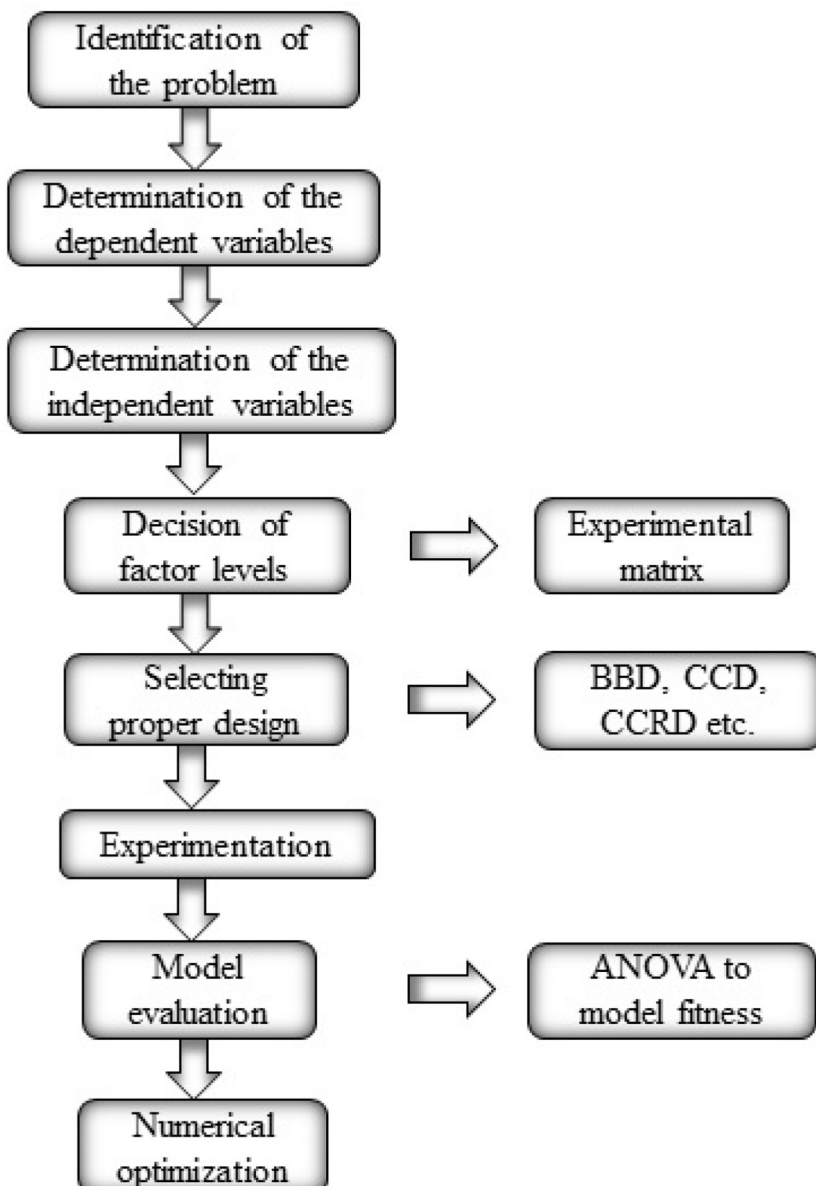


Fig. 2. RSM sequence for the engine response optimization.

Fig. 2 illustrates how the RSM approach is applied. The values of the input variables, including the lowest and maximum, that are intended to be studied in the research should be established. Because of the investigation, the experiments are carried out with the necessary data measurements by selecting the response parameters that are intended to be evaluated. A RSM plan is developed, and experimental data sets are produced after the determination of the dependent and independent variables. If all circumstances are the same, the constructed experimental sets are run in accordance with the input parameters indicated. Numerical optimization is the RSM method's last phase. The targeted criteria are entered into the response variables during optimization, and the ideal independent variables are found. In this research, the Design Expert-12 software was used to apply the RSM methodology. Engine load and hydrogen share were used as RSM input parameters.

3.6.1. Design of experiment

For creating an experimental design matrix, a typical Central Composite Design (CCD) model was chosen. It produces accurate results with the fewest possible run orders. The three numerical input factors are shown in **Table 5** together with their input levels (high +1, 0, and low -1). This results in 25 runs with four centre points for each block. The necessary dependent variables are input from the experimentation and are shown in **Table 6** once the run order has been constructed. The input components chosen were hydrogen premixing and engine load, while the output responses chosen were combustion (peak in-cylinder pressure), performance (BTE, BSEC), and emission (HC, CO, NO_x, smoke opacity, and exhaust gas temperature) parameters. This research tries to maximize the BTE and minimize the remaining output variables by optimizing the input variables.

3.6.2. Features of RSM

The RSM must determine how an input factor interacts with a collection of responses. Additionally, it optimizes the ideal output solutions by maximizing or reducing the process parameters within predefined limitations. In order to assess the model equality built for each response, an ANOVA was utilized. Equation (3) provides the cubic model that was used to derive the response parameters based on the variables provided in the RSM. The input parameter in the model is x_i , the response is y , the constant coefficient is b_0 , the regression coefficients are b_i , b_{ii} , and b_{iii} , and the cubic coefficient is b_{ij} . The RSM-created design includes a total of 25 tests. The RSM model optimizes the input factors of hydrogen premixing and engine load with high precision.

$$y = b_0 + \sum_{i=1}^k b_i x_i + \sum_{i=1}^k b_{ii} x_i^2 + \sum_{i=1}^k b_{iii} x_i^3 + \sum_{i=1}^k \sum_{j=1, j < i}^k b_{ij} x_i x_j \quad (3)$$

Equations (4)–(6) used to get the RSM coefficients are:

$$\text{Correlation coefficient } (R^2) = 1 - \frac{\text{Sum of Squares}_{\text{Residual}}}{\text{Sum of Squares}_{\text{Residual}} + \text{Sum of Squares}_{\text{Model}}} \quad (4)$$

$$\text{Adj. } R^2 = \frac{\text{Sum of Squares}_{\text{Residual}}}{df_{\text{Residual}}} / \left(\frac{\text{Sum of Squares}_{\text{Residual}} + \text{Sum of Squares}_{\text{Model}}}{df_{\text{Residual}} + df_{\text{Model}}} \right) \quad (5)$$

$$\text{Pred. } R^2 = 1 - \frac{\text{Predicted Residual Sum of Squares}}{\text{Sum of Squares}_{\text{Residual}} + \text{Sum of Squares}_{\text{Model}}} \quad (6)$$

The relative importance of each variable was assessed using the ANOVA **Table 7** results, and a statistically significant regression was found for the peak in-cylinder pressure, BTE, BSEC, HC, CO, NO_x, smoke opacity, and EGT. The adj R^2 value indicates that correlation coefficients are valid and describes the influence of hydrogen proportion for operation with a 40% ammonia biodiesel energy share. The constructed regression models for each response are shown in **Table 8** (equation 7–14), where A stands for load and B for hydrogen premixing percentage in the operation of 40% ammonia biodiesel. Overall, the RSM-based regression analysis reveals that hydrogen proportion behavior about the experiment's conditions was well predicted.

3.6.3. Desirability function approach (DFA)

The numerous regression equations from the RSM model are optimized using the DFA, which is often employed in many realistic real-world applications. All the output responses are combined to form the nondimensional variable known as the individual desirability (P_i) value. The range of P_i numbers is 0 to 1. When the response variable reaches the target or goal values, the desirability approaches 1. If the response is outside of the acceptable range, the desirability approaches near 0. Each response's objective may be maximized, minimized, targeted, in the range, or equal to, depending on how the problem is presented. The objective functions of each response are estimated by equations (15)–18.

the goal of minimum condition, $P_i = 1$ while $Z_i \leq A_i$; $P_i = 0$ as $Z_i \geq B_i$

Table 5
RSM input levels.

| Independent variables | Codes | Levels | | |
|--------------------------------|-------|---------|-----------|---------|
| | | -1(low) | 0(medium) | 1(High) |
| Engine load | A | 20 | 50 | 100 |
| 40% NH ₃ + Hydrogen | B | 0 | 10 | 20 |

Table 6
RSM experimental design.

| Std | Run | Load (%) | 40%AEF + Hydrogen (%) |
|-----|-----|----------|-----------------------|
| 14 | 1 | 20 | 0 |
| 16 | 2 | 20 | 5 |
| 1 | 3 | 20 | 10 |
| 22 | 4 | 20 | 15 |
| 19 | 5 | 20 | 20 |
| 2 | 6 | 40 | 0 |
| 24 | 7 | 40 | 5 |
| 8 | 8 | 40 | 10 |
| 10 | 9 | 40 | 15 |
| 9 | 10 | 40 | 20 |
| 15 | 11 | 60 | 0 |
| 13 | 12 | 60 | 5 |
| 21 | 13 | 60 | 10 |
| 11 | 14 | 60 | 15 |
| 18 | 15 | 60 | 20 |
| 4 | 16 | 80 | 0 |
| 6 | 17 | 80 | 5 |
| 25 | 18 | 80 | 10 |
| 3 | 19 | 80 | 15 |
| 17 | 20 | 80 | 20 |
| 5 | 21 | 100 | 0 |
| 12 | 22 | 100 | 5 |
| 20 | 23 | 100 | 10 |
| 7 | 24 | 100 | 15 |
| 23 | 25 | 100 | 20 |

Table 7
RSM ANOVA results.

| Source/Model | Peak in-cylinder pressure | BTE | BSEC | HC | CO | NO _x | Smoke opacity | EGT |
|--------------------------|---------------------------|--------|---------|--------|--------|-----------------|---------------|--------|
| Std. Dev. | 0.5939 | 0.3354 | 0.2574 | 1.43 | 0.0025 | 4.79 | 0.6595 | 8.65 |
| Mean | 60.49 | 26.93 | 15.34 | 67.96 | 0.1339 | 388.44 | 16.71 | 292.6 |
| C.V. % | 0.9818 | 1.25 | 1.68 | 2.1 | 1.87 | 1.23 | 3.95 | 2.96 |
| R ² | 0.996 | 0.999 | 0.997 | 0.9957 | 0.998 | 0.9998 | 0.9989 | 0.9952 |
| Adjusted R ² | 0.9935 | 0.9977 | 0.9963 | 0.9946 | 0.9968 | 0.9996 | 0.9973 | 0.9939 |
| Predicted R ² | 0.9807 | 0.9946 | 0.9942 | 0.9925 | 0.9941 | 0.9993 | 0.9835 | 0.992 |
| Adeq. Precision | 67.2139 | 79.19 | 104.827 | 93.576 | 97.835 | 238.391 | 76.2712 | 85.342 |

Table 8
Engine behavior regression equation for Hydrogen premixing.

| Response | Regression equation | Equation |
|---------------------------|--|----------|
| Peak in-cylinder pressure | 60.88 + 8.32 A+3.53 B + 0.8299 AB-0.4542 A ² -0.3309 B ² -0.0522 A ² B-0.6785 AB ² +2.04 A ³ -0.5264 B ³ | (7) |
| BTE | 29.30 + 10.00 A+2.31 B + 1.70 AB-5.69 A ² +1.74 B ² -0.3126 A ² B-0.5434 AB ² -0.7600 A ³ -0.8827 B ³ -0.5151 A ² B ² +0.3320 A ³ B-1.35 AB ³ +1.01 A ⁴ -1.63 B ⁴ | (8) |
| BSEC | 13.94 - 5.52 A-1.09 B-0.1492 AB+2.53 A ² +0.2531 B ² | (9) |
| HC | 62.96 - 25.28 A-7.48 B + 2.24 AB+9.14 A ² +0.8571 B ² | (10) |
| CO | 0.1223 -0.0545 A-0.0248 B + 0.0101 AB+0.0190 A ² +0.0042 B ² -0.0031 A ² B+0.0027 AB ² -0.0025 A ³ +0.0053 B ³ | (11) |
| NO _x | 351.41 + 379.92 A+29.89 B + 30.64 AB+74.80 A ² -0.7429 B ² +3.89 A ² B+0.6857 AB ² -54.67 A ³ | (12) |
| Smoke opacity | 13.37 + 9.23 A-2.02 B-1.12 AB-2.33 A ² -2.28 B ² -0.9543 A ² B+0.3714 AB ² +7.87 A ³ +0.9600 B ³ +0.4816 A ² B ² -0.8800 A ³ B+0.9867 AB ³ +10.77 A ⁴ +2.24 B ⁴ | (13) |
| EGT | 318.43 + 146.44 A+34.36 B + 18.40 AB-48.06 A ² -3.60 B ² | (14) |

$$P_i = \frac{(B_i - Z_i)^{wt}}{B_i - Z_i} \text{ if } A_i < Z_i < B_i \quad (15)$$

The goal of maximum, $P_i = 0$ while $Z_i \leq A_i$; $P_i = 1$ as $Z_i \geq B_i$

$$P_i = \frac{(Z_i - A_i)^{wt}}{B_i - A_i} \text{ if } A_i < Z_i < B_i \quad (16)$$

The goal of target, $P_i = 0$ while $Z_i < A_i$; $Z_i > B_i$

$$P_i = \frac{(Z_i - A_i)^{wt_i}}{T_i - L_i} \text{ if } A_i < Z_i < T_i \quad (17)$$

$$P_i = \frac{(Z_i - B_i)^{wt_i}}{T_i - B_i} \text{ if } A_i < Z_i < B_i \quad (18)$$

where i is the number of responses, Z is the response's value, A and B are each response's lower and higher limits, T is the target value of the response, and wt is the weight of the response. The overall desirability (P) is calculated in equation (19) as follows:

$$P = \sqrt[n]{P_1 + P_2 + P_3 \dots P_n} \quad (19)$$

Here, n represents the response number.

Fig. 3 depicts the sequence of the MATLAB technique, from variable definition to neuron layer construction to neuron training to evaluating the trained neuron model using significant components of the source code. The next section discusses the combustion, performance, and emission phenomena caused by hydrogen enrichment in comparison to 40% ammonia and 60% biodiesel outcomes.

4. Results and discussion

4.1. Combustion characteristics

4.1.1. Peak in-Cylinder pressure

The relationship between in-cylinder pressure fluctuation and crank angle is crucial for identifying quantifiable, useful information about the engine's combustion process. In the operation of the hydrogen-enriched ammonia/biodiesel dual fuel RCCI, the peak cylinder pressure was somewhat advanced. Ammonia cannot be used as a fuel because of the poor burning velocity of NH₃ with air flames. A feasible method for attaining carbon-free combustion and flame intensification at the same time is hydrogen addition. The laminar burning velocity exponentially rises with hydrogen energy due to hydrogen's reactivity. Fig. 4 illustrates how the cylinder pressure fluctuates with respect to crank angle for different hydrogen-enriched ammonia-biodiesel operations. At peak load conditions, the peak pressure values for all the operations are 65.87, 68.43, 70.6, 72.04, and 75.83 bar with 0%, 5%, 10%, 15%, and 20% hydrogen enrichment operations. In contrast to ammonia biodiesel dual fuel operation without hydrogen enrichment, the engine's cylinder pressure was increased by 3.89%, 7.18%, 9.37%, and 15.12%. Fuel combustion is enhanced when H₂ is enriched with ammonia/biodiesel because it causes a reduced ignition delay with a greater in-cylinder pressure. The degree of ignition delay shortens with increasing cylinder temperatures, more precisely at greater loads; therefore, the combustion gradually progresses bTDC. The

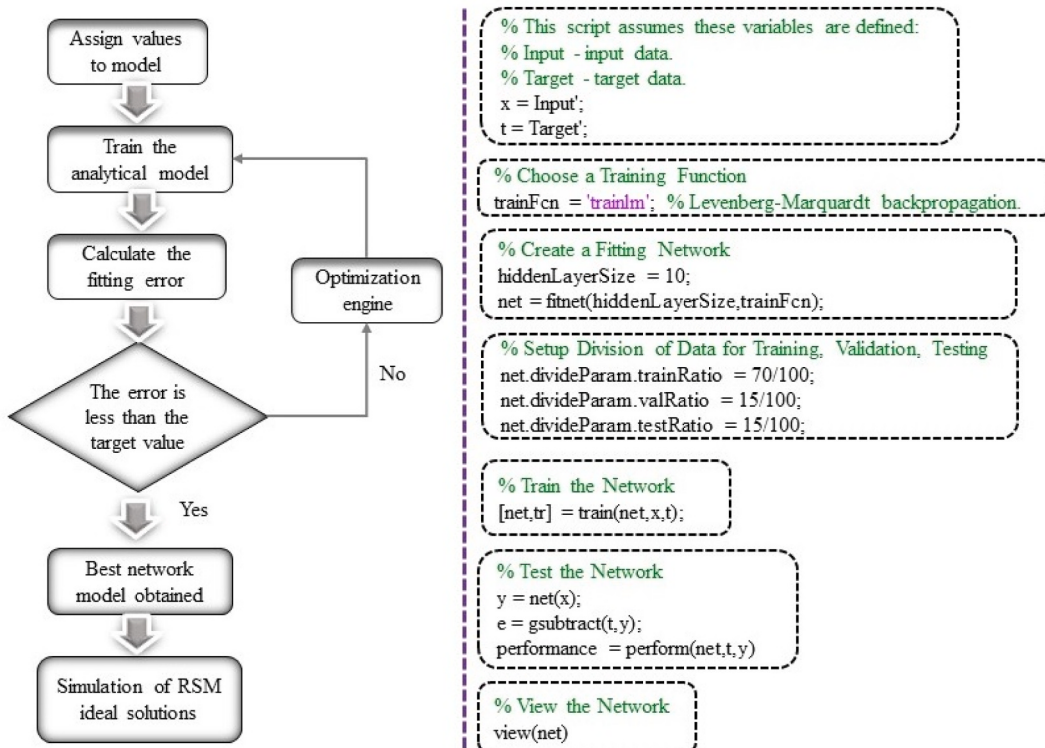


Fig. 3. MATLAB algorithm order for the response prediction of the engine behavior model.

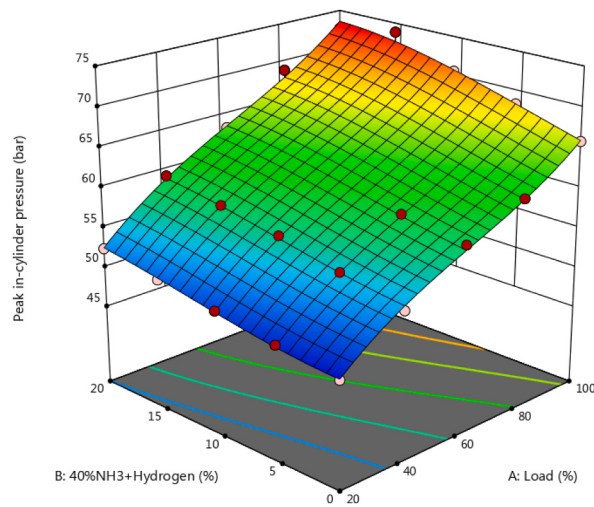


Fig. 4. Interaction of load and gaseous fuel premixing with peak in-cylinder pressure.

phenomenon that causes pressure to increase is further enhanced by the addition of hydrogen to ammonia/biodiesel combustion. Therefore, it is claimed that the increased rate of hydrogen enrichment enhances flame propagation, results in advancements in combustion, and shortens the overall combustion duration. The combustion of hydrogen, ammonia, and biodiesel fuel increased the amount of energy dissipated in the engine and decreased the phenomenon of ammonia escapes. On the other hand, the biodiesel fuel-bound oxygen managed to reduce air intake for every increase in energy share of ammonia and hydrogen flowing into the combustion process. In comparison to the burning of hydrogen-enriched ammonia and biodiesel, the plain ammonia-biodiesel RCCI mode produced lower pressure. The fuel's peak cylinder pressure was raised by the addition of hydrogen. In comparison to the ammonia/biodiesel operation, the peak cylinder pressures for H₂ enrichment occurred somewhat delayed. With the addition of hydrogen with the ammonia premixed biodiesel combustion, the peak in-cylinder pressure is advanced, and the peak pressure rise rate is increased. The highest peak of in-cylinder pressure was attained for 20% hydrogen enrichment operation; hence, the studies were restricted to 20% hydrogen enrichment, and higher concentrations of hydrogen may cause engine components to be damaged.

4.2. Performance characteristics

4.2.1. Brake thermal efficiency

BTE is the ratio of useable work received at the crankshaft to the amount of fuel used to produce that work [76,77]. The engine's BTE is determined by the heating value and the physicochemical characteristics of the test fuel. Fig. 5 illustrates the BTE interaction of engine load with respect to fuels. As hydrogen is introduced through the intake manifold with ammonia, the thermal efficiency improves regardless of load. At full load, the engine's BTE was observed to be 31.1%, 32.41%, 33.38%, 34.72%, and 35.93% with 0%, 5%, 10%, 15%, and 20% hydrogen energy shares, respectively. In contrast to 40% ammonia-biodiesel dual fuel operation without

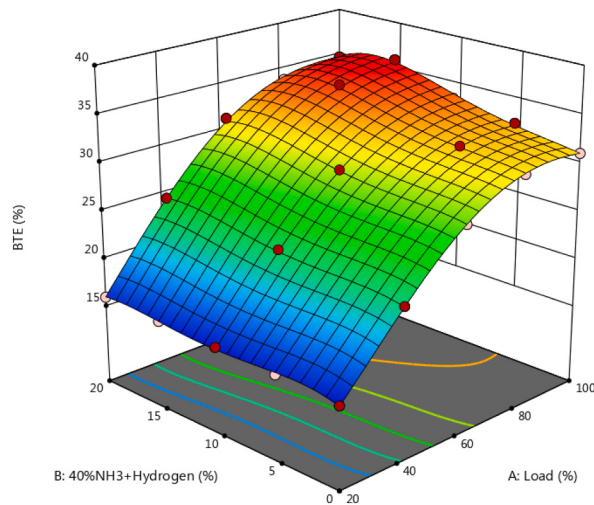


Fig. 5. Interaction of load and gaseous fuel premixing with BTE.

hydrogen enrichment, the engine's BTE was enhanced by 4.17%, 7.29%, 11.58%, and 15.49%. Premixed ammonia-hydrogen with air is entering the combustion chamber; pilot injected biodiesel serves as an ignition source for the premixed charge, which releases a greater amount of heat during the premixed combustion. Because of hydrogen's fast flame speed, the flame goes to the end of the combustion chamber, where the flame formed by biodiesel-ammonia dual fuel operation may not reach, the combustion of ammonia is hindered, the ammonia escape phenomenon happens, and the ammonia mixture close to the cylinder walls cannot burn, leading to misfire. As a result, the combustion efficiency increases, which enhances thermal efficiency.

4.2.2. Brake specific energy consumption

The fraction of energy provided to generate unit engine power is known as the BSEC. The BSEC, which is based on fuel characteristics, is a gauge of how efficiently an engine uses energy [78]. Fig. 6 illustrates how BSEC values vary based on the various hydrogen percentages and engine loads. However, BSEC is considered a more realistic indicator for evaluating the performance of an engine running on various fuels. The BSEC is higher with ammonia/biodiesel dual fuel operation as a result of the lower calorific value of the fuel mixture. A maximum BSEC of 23 MJ/kWh was attained with 40% ammonia-biodiesel dual fuel operation. This is because the combustion rate of fuel was reduced by ammonia energy, which increased the BSEC. Because of the reduced heating properties of NH₃, a higher quantity of fuel was required to sustain the same load. At full load, the engine's BSEC was found to be 12.5 MJ/kWh, 11.75 MJ/kWh, 11.05 MJ/kWh, 10.38 MJ/kWh, and 9.76 MJ/kWh, with 0%, 5%, 10%, 15%, and 20% hydrogen energy shares, respectively. In contrast to 40% ammonia-biodiesel dual fuel operation without hydrogen enrichment, the engine's BSEC was reduced by 6%, 11.64%, 16.94%, and 21.92%. Hydrogen enrichment of 20% exhibits the minimal BSEC, which is attributed to the proper mixing of hydrogen with ammonia and air. Hydrogen ignites the ammonia, reduces the ammonia escape phenomenon, and helps to achieve close to complete combustion. It can be noticed that BSEC normally shows a reduction as the load increases. The in-cylinder wall temperatures rose, the ignition delay shortened, and the combustion progressed consequently, leading to diminishing trends in the BSEC. The reduced volumetric calorific value of hydrogen and ammonia/biodiesel fuel may be responsible for the decrease in BSEC during hydrogen enrichment. As the hydrogen ratio rises, the mixture's stoichiometric air-to-fuel ratio rises since hydrogen has a higher stoichiometric air-to-fuel ratio, even though ammonia has a lesser stoichiometric ratio. Further premixing of gaseous fuel into the combustion leads to a reduction in the intake of oxygen. Therefore, the experiment was limited to 20% hydrogen premixing with a 40% premixed ammonia-biodiesel operation.

4.3. Emission characteristics

4.3.1. Hydrocarbon emission

Greater HC emissions relate to the biodiesel concentrated combustion process due to higher viscosity and poor atomization, which leads to incomplete combustion [79]. At peak load conditions, the engine's HC emission was observed to be 53 ppm, 50 ppm, 46 ppm, 42 ppm, and 40 ppm with 0%, 5%, 10%, 15%, and 20% hydrogen energy shares, respectively. In contrast to 40% ammonia-biodiesel dual fuel operation without hydrogen addition, the engine's HC emission was reduced by 5.6%, 13.2%, 20.75%, and 24.53%. Lower HC emissions were produced by the hydrogen-enriched ammonia/biodiesel dual fuel RCCI, which improved combustion. The HC emissions of the hydrogen enrichment were discovered to be lower than those of the ammonia/biodiesel dual fuel operation under all operating circumstances, as illustrated in Fig. 7. During the ammonia/biodiesel dual fuel operation, the amount of HC emission was higher at different engine loads. Because ammonia has a lower diffusivity than biodiesel, it produced a biodiesel-richer mixture in the

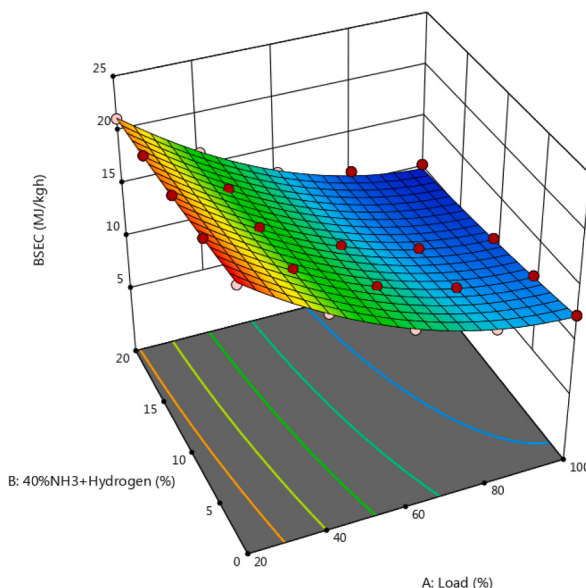


Fig. 6. Interaction of load and gaseous fuel premixing with BSEC.

combustion chamber, and an improper air-to-fuel mixture increased HC emission. The fuel absorbed heat as a result of ammonia's latent heat of evaporation, which decreased in-cylinder temperatures and retarded the oxidation of HC. Therefore, adding hydrogen enrichment to ammonia-biodiesel makes the better fuel-air combination burn more completely and more quickly, which decreases the amount of unburned hydrocarbon emissions since hydrogen's quicker flame propagation and higher diffusivity speed up combustion. The availability of oxygen in the air is reduced with greater gaseous hydrogen/ammonia induction. Thus, the local air-to-fuel ratios were reduced. This might be the reason to limit the hydrogen enrichment to 20%.

4.3.2. Carbon monoxide emission

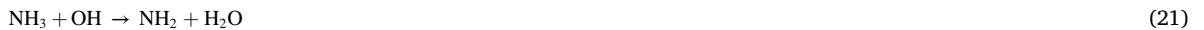
The lack of carbon in the H₂ fuel accounts for the further decrease in CO in the hydrogen-enriched ammonia/biodiesel dual fuel engine. At full load, the engine's CO emissions were observed to be 0.103% vol, 0.095% vol, 0.087% vol, 0.08% vol, and 0.074% vol, with 0%, 5%, 10%, 15%, and 20% hydrogen energy shares, respectively. In contrast to 40% ammonia-biodiesel dual fuel operation without hydrogen addition, the engine's CO emissions were reduced by 7.76%, 15.53%, 22.33%, and 28.16%. The CO emissions of the hydrogen enrichment were discovered to be lower than those of the ammonia/biodiesel dual fuel combustion under all operating circumstances, as illustrated in Fig. 8. The biodiesel O₂ concentration rose noticeably at 100% load, which contributed to the decrease in CO production rate. H₂ addition may lower CO emissions since the hydrogen in the fuel mixture further reduces the carbon/hydrogen ratio composition. Additionally, the superior homogeneity of the combustible mixture produced by hydrogen's higher diffusivities compared to other fuels allows for more oxygen to be accessible to accelerate combustion, causing a quicker combustion response within the combustion chamber. The ammonia/biodiesel that produce higher CO emissions as a result of incomplete combustion have the potential for flame quenching. Additionally, OH radicals formed in the combustion of hydrogen increased the conversion of carbon monoxide to carbon dioxide, leading to lower CO emissions.

4.3.3. Nitrogen oxide emission

The temperature, resident time of combustion, and oxygen content of combustion have a significant impact on NO_x generation [80, 81]. Greater oxygen concentrations and higher combustion temperatures promote the generation of thermal nitrogen oxide. The oxidation of nitrogen in the air and fuel is the main cause of NO_x generation, according to the principle of combustion-science theory. At full load, the engine's NO_x emissions were observed to be 682 ppm, 718 ppm, 750 ppm, 786 ppm, and 818 ppm with 0%, 5%, 10%, 15%, and 20% hydrogen energy shares, respectively. In contrast to 40% ammonia-biodiesel dual fuel operation without hydrogen enrichment, the engine's NO_x emissions increased by 5.23%, 9.97%, 15.25%, and 19.94%. The NO_x emissions of the hydrogen enrichment were discovered to be higher than those of the ammonia/biodiesel fuel combustion under all operating circumstances, as illustrated in Fig. 9.

Fuel NO_x formation.

The principal oxidation paths of NH₃ decomposition of H abstraction reactions are (equation (20) and (21)):



NH₂ to NH oxidation paths of H abstraction reactions (equation (22) and (23))

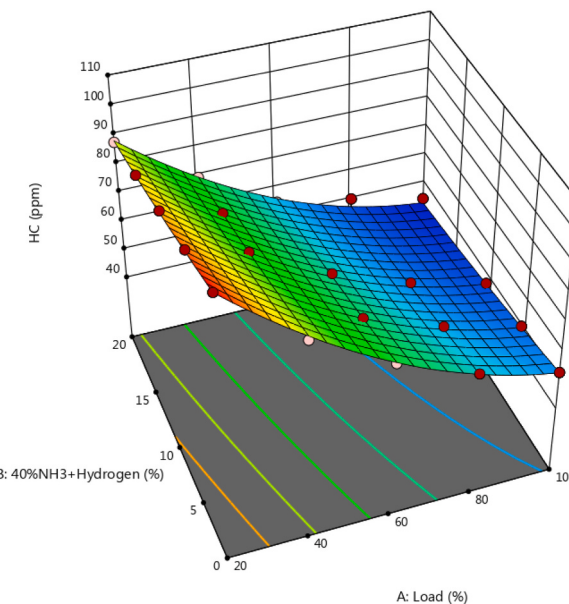


Fig. 7. Interaction of load and gaseous fuel premixing with HC.

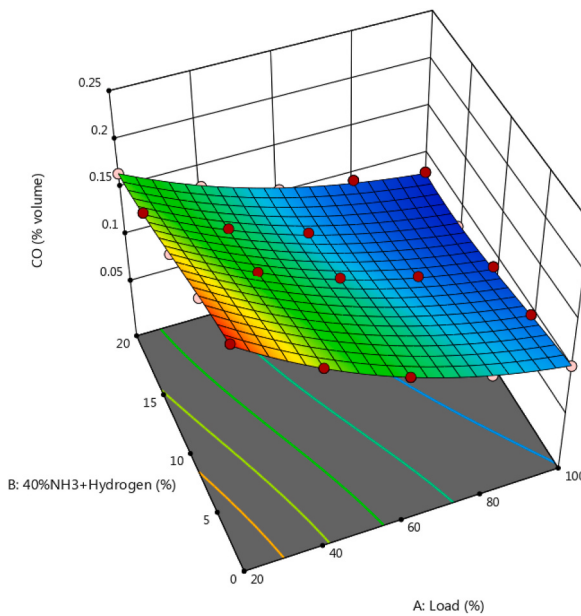


Fig. 8. Interaction of load and gaseous fuel premixing with CO.

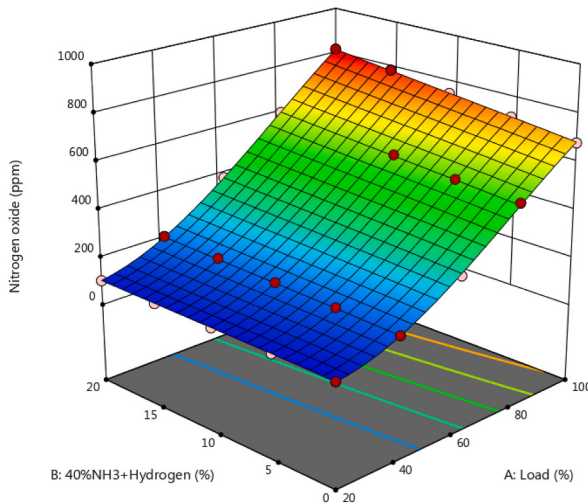


Fig. 9. Interaction of load and gaseous fuel premixing with NO_x.



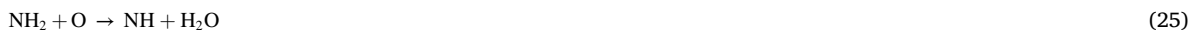
Lean equivalency ratio facilitates the formation of NH to NO with O and OH pool groups. The interaction ammonia radicals with OH, HO₂, O and O₂ to create NO via HNO and H₂NO are the foremost mechanism for the creation of fuel NO_x during oxidation.

One of the most significant reactions that lead to the formation of intermediate HNO species is (equation (24)):



this is the majority responsive reaction in NO formation.

The above reaction has a branching reaction for NH₂ consumption (equation (25)):



However, it is less favored at higher combustion temperatures. As a result, it accounts for a negligible portion of NH₂ consumption, The following are examples of NH radical reactions with O, O₂ and OH to form NO:



equation (26) and (27) engage the reactions of NH with active radicals for intermediate species of HNO. equation (28) and (29) engage the reactions of NH with active radicals for direct NO decomposition [82].

The intermediate products of HNO to NO decomposition reactions are as follows (equation (30)–(32)):



In addition, adding hydrogen to the ammonia/biodiesel enhanced the NO_x emissions because the premixed combustion phase increased as a result of the H_2 induction, which is linked to high NO_x emissions and an increase in flame temperature. Additionally, increasing the flow rates of hydrogen gas led to an overall increase in NO_x emissions. The resultant NO_x emissions at all engine loads increased significantly because of the addition of hydrogen to ammonia-biodiesel. Owing to the greater calorific value of H_2 fuel, a higher amount of heat is emitted, which is the cause of this trend. When using ammonia and biodiesel dual fuel operation, the NO_x emissions from the burned fuel were greatly decreased. This happened because of the induction of ammonia, which forms the thermal stratification inside the cylinder and ammonia absorbs heat, lowering the cylinder overall temperature. As a result of NO generation was decreased for the ammonia/biodiesel dual fuel operation.

4.3.4. Smoke opacity

Inadequate air to fuel mixture in the combustion chamber, inefficient fuel combustion, a lack of oxygen, and a low combustion temperature all contribute to incomplete combustion of the fuel, which results in smoke production [83]. At full load, the engine's smoke opacity was observed to be 42.5%, 41.1%, 39.7%, 35.3%, and 37.1% with 0%, 5%, 10%, 15%, and 20% hydrogen energy shares, respectively. In contrast to 40% ammonia-biodiesel dual fuel operation without hydrogen addition, the engine's smoke opacity was reduced by 3.29%, 6.59%, 16.94%, and 12.71%. Fig. 10 shows that for each engine load, the ammonia/biodiesel dual fuel with 20% H_2 enrichment exhibits a higher reduction in smoke than the ammonia/biodiesel operation. Biodiesel has a favorable impact on smoke emissions because it doesn't evaporate completely. Additionally, when engine load increased, the smoke opacity emissions measured for the test fuel significantly increased. The quantity of fuel consumption rises as load increases, and the fact that the injected fuel is not entirely burned causes smoke emissions to rise as well. In literature, similar outcomes were attained. Owing to the increased mass diffusivity of hydrogen, which combines with oxygen more quickly and burns more readily during the premixed combustion phase, less smoke is produced. Biodiesel is the sole source of smoke from hydrogen, ammonia, and biodiesel operations because hydrogen starts burning before the biodiesel mixes properly with air due to its high flame speed. More biodiesel is injected into the cylinder as the load rises; combustion inside the cylinder is incomplete, which increases smoke opacity for ammonia biodiesel operation at higher loads.

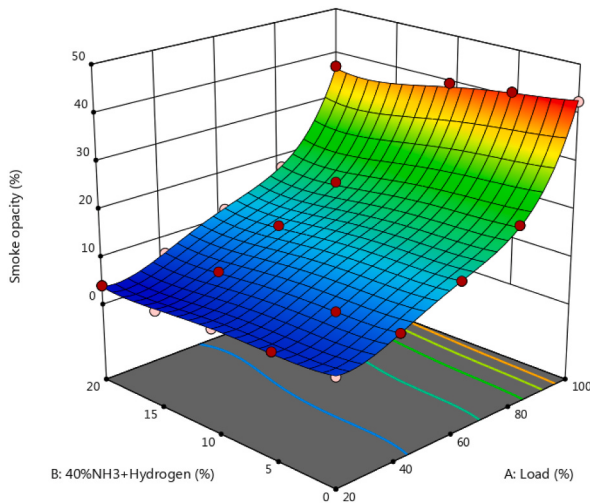


Fig. 10. Interaction of load and gaseous fuel premixing with smoke opacity.

4.3.5. Exhaust gas temperature

The exhaust gas temperature represents how quickly heat is emitted in the combustion chamber. At full load, the engine's exhaust gas temperature (EGT) was observed to be 458°C, 434°C, 419°C, 396 °C, and 378°C with 0%, 5%, 10%, 15%, and 20% hydrogen energy shares, respectively. In contrast to 40% ammonia-biodiesel dual fuel operation without hydrogen addition, the engine's exhaust temperature was reduced by 5.25%, 8.51%, 13.53%, and 17.47%. A slow-burning fuel produces a lengthy afterburning phase, which raises the temperature of the exhaust gas. Additionally, a large quenching distance prevents efficient heat transfer from the cylinder wall, raising the temperature of the exhaust gas as a result. Fig. 11 illustrates these two effects, which are dominant in ammonia combustion. However, when the hydrogen enrichment level in the ammonia/biodiesel increases, the burning efficiency increases and the EGT decreases [84]. The EGT is decreased by increasing the hydrogen proportion since it accelerates combustion and shortens the quenching distance. This impact becomes more apparent with increasing load because the load rises, which in turn causes the EGT to rise. However, it is shown that ammonia/biodiesel dual fuel operation has a higher EGT. This may be because of the lengthy afterburning time, which permits some mass to burn during the late combustion phase and increases the EGT.

5. ANN engine response model

The most effective method for predicting the behavior of engineering systems is a non-linear ANN methodology. The collected experimental data was used in this study to create an ANN-based response model. To facilitate training, validation, and testing, The data was separated into three distinct sets at random. 75% of the data was chosen at random for training, and the remaining samples were equally divided between testing and validation. The network in this case is made up of an output layer with one dependent variable, a hidden layer with 10 neurons, and an input layer with two independent variables. To forecast the dependent variables of peak in-cylinder pressure, BTE, BSEC, HC, CO, NO_x, smoke, and EGT, a total of 8 ANN models have been created. The TRAINLM function, also known as the Levenberg-Marquardt back propagation method, was used with the framed network. The TRANSIG algorithm assists in identifying the output parameter based on the input variable. An optimal neuron size of 10 was discovered via trial and error.

Additionally, the ANN model performed recurrent training, testing, and validation for each of the responses. The performance of weights and bias values is chosen for the network based on the MSE value. Based on the findings, the interpretation of the experimental data and the anticipated data has been assessed using the R value shown in Table 9. The created ANN model may be able to predict the real-time reactions that happened throughout the experiment, as the obtained results are extremely close to 1. Furthermore, the tests that were carried out and the corresponding results were enough to provide a highly fitting correlation coefficient. Additionally, the RSM optimization outperforms the ANN. From this, it is possible to use the constructed ANN model to predict engine reactions in relation to hydrogen enrichment percentage.

6. Optimality of the hydrogen premixing

The RSM technique was used to determine the ideal premixing percentage of hydrogen as an additive in 40% ammonia biodiesel dual fuel operation, depending on the highest anticipated CI engine emission levels and performance. The needed engine response behavior requirements are specified in order to achieve the location of the best premixing, and specifics are given in Table 10. The goal of the load is changed to target, and values are entered as required load conditions while other criteria remain unchanged. Each response's and factor's degree of relevance is given equal weight. BTE and peak in-cylinder pressure are regarded as being at their greatest levels for the purpose of determining responses, while the remaining BSEC, CO, HC, and smoke are at their lowest levels. The experimental results are used to determine the minimum and maximum response ranges and factor ranges. Table 11 presents the optimized hydrogen share generated from the RSM determined using the desirability method. The surface map makes it evident how the overall ideal value changes in relation to the ammonia and hydrogen content and the impact of engine loads. The greatest BTE in the total desired factor was attained by adding 17.12% hydrogen to the 40% ammonia-fueled biodiesel operation mode at full load. Additionally, the ANN model-based combustion pressure and performance simulation results are shown in Table 12, and Table 13 represents the emission results.

7. Experimental validation and comparison of calibrated control map

Experiments are done on the engine under specific working conditions to verify that the optimized, calibrated maps are made with the DNN model-based method. For each working condition, three measures are taken. The mean value of the test findings is analyzed to ensure the accuracy of the optimization outcomes and to evaluate variations. Table 14 compares the engine characteristics of RSM's and ANN's test values with experimental values. Also, the model prediction values at 50% of the load that had been tested were experimentally validated. The best-calibrated map gives responses that are almost the same as the validated results. Furthermore, the relative difference between the measured and predicted values of the optimized map illustrates the calibration's precision.

8. Conclusion

In this study, the CI engine was operated at a perpetually consistent rpm of 1500 rpm with LRF such as ammonia and hydrogen being port injected and HRF biodiesel being directly injected. The energy share of ammonia in premixing is set at 40%; the hydrogen enrichment to the 40% ammonia premixing varies from 5 to 20%; and the rest of the energy is biodiesel. The RSM and ANN models are used to make an exact regression model for the results of the experiments and to map out the best amount of hydrogen for different load conditions. The research findings are as follows:

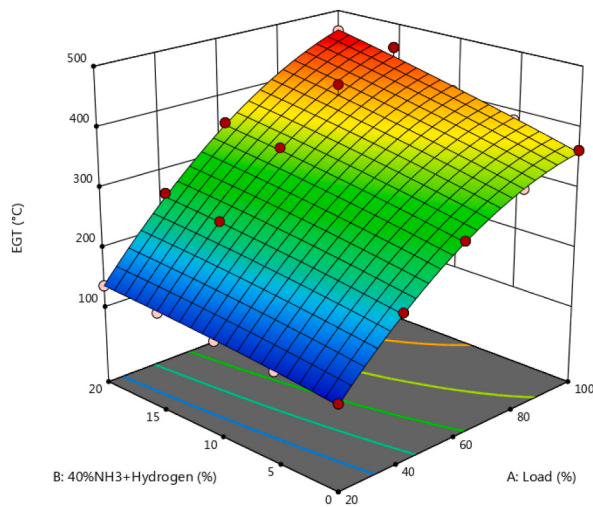


Fig. 11. Interaction of load and gaseous fuel premixing with EGT.

Table 9

Error analysis of ANN based prediction results.

| Responses | Correlation coefficient R | | |
|---------------------------|---------------------------|--------|------------|
| | Training | Test | Validation |
| Peak in-cylinder pressure | 0.9947 | 0.9999 | 0.9991 |
| BTE | 0.9867 | 0.9965 | 0.9973 |
| BSEC | 0.9996 | 0.9761 | 0.9988 |
| HC | 0.9974 | 0.9387 | 0.9962 |
| CO | 0.992 | 0.974 | 0.9996 |
| NO _x | 0.9923 | 0.9636 | 0.9893 |
| Smoke opacity | 1 | 0.9944 | 0.9798 |
| EGT | 1 | 0.9976 | 0.9781 |

Table 10

RSM optimization criteria.

| Parameters | Goal | Lower Limit | Upper Limit | Lower Weight | Upper Weight | Importance |
|--------------------------------|-------------|-------------|-------------|--------------|--------------|------------|
| A: Load | target | 20 | 100 | 1 | 1 | 3 |
| B:40%NH ₃ +Hydrogen | is in range | 0 | 20 | 1 | 1 | 3 |
| Peak in-cylinder pressure | is in range | 48.21 | 73.83 | 0.1 | 1 | 3 |
| BTE | maximize | 15.14 | 35.93 | 0.1 | 1 | 3 |
| BSEC | is in range | 9.76 | 23 | 1 | 0.1 | 3 |
| HC | is in range | 41 | 108 | 1 | 0.1 | 3 |
| CO | is in range | 0.074 | 0.234 | 1 | 0.1 | 3 |
| NO _x | is in range | 96 | 818 | 1 | 0.1 | 3 |
| Smoke opacity | is in range | 3.4 | 42.5 | 1 | 0.1 | 3 |
| EGT | is in range | 107 | 464 | 1 | 0.1 | 3 |

Table 11

RSM optimized output for different load condition.

| Load | 40%NH ₃ +Hydrogen | Peak in-cylinder pressure | BTE | BSEC | HC | CO | NO _x | Smoke opacity | EGT | Desirability |
|------|------------------------------|---------------------------|-------|-------|-------|------|-----------------|---------------|-----|--------------|
| 20 | 14.77 | 51.363 | 15.73 | 21.6 | 92.94 | 0.18 | 102 | 3.865 | 131 | 1 |
| 30 | 18.75 | 55.834 | 20.42 | 18.84 | 79.7 | 0.15 | 140 | 3.752 | 197 | 1 |
| 40 | 18.93 | 58.941 | 24.42 | 16.57 | 70.14 | 0.13 | 203 | 6.63 | 255 | 0.9899 |
| 50 | 17.94 | 61.016 | 28.18 | 14.8 | 64 | 0.12 | 280 | 9.184 | 300 | 1 |
| 60 | 16.43 | 62.5 | 30.68 | 13.46 | 59.43 | 0.11 | 366 | 12.047 | 335 | 0.9799 |
| 70 | 14.42 | 64.474 | 32.78 | 12.27 | 54.32 | 0.1 | 467 | 14.411 | 369 | 1 |
| 80 | 15.58 | 66.915 | 34.45 | 11.3 | 49.64 | 0.09 | 576 | 17.418 | 401 | 0.9879 |
| 90 | 13.23 | 68.949 | 34.77 | 10.87 | 47.36 | 0.09 | 673 | 24.389 | 416 | 0.9988 |
| 100 | 17.12 | 73.121 | 35.86 | 10.21 | 43.58 | 0.08 | 797 | 35.925 | 452 | 0.999 |

Table 12
ANN combustion and performance simulation results.

| Load | 40%NH ₃ +Hydrogen | Peak in-cylinder pressure | | BTE | BSEC |
|------|------------------------------|---------------------------|------------|-------|-------|
| | | Simulation | Simulation | | |
| 20 | 14.77 | 50.72 | | 16.5 | 21.60 |
| 30 | 18.75 | 54.77 | | 20.82 | 19.40 |
| 40 | 18.93 | 58.92 | | 22.93 | 16.40 |
| 50 | 17.94 | 61.04 | | 27.37 | 14.81 |
| 60 | 16.43 | 61.82 | | 29.99 | 13.00 |
| 70 | 14.42 | 63.25 | | 32.18 | 12.40 |
| 80 | 15.58 | 65.72 | | 33.8 | 11.70 |
| 90 | 13.23 | 67.96 | | 35.21 | 10.57 |
| 100 | 17.12 | 71.45 | | 35.81 | 9.80 |

Table 13
ANN emission simulation results.

| Load | 40%NH ₃ +Hydrogen | HC | CO | | NO _x | Smoke opacity | | EGT |
|------|------------------------------|-------|------------|------------|-----------------|---------------|------------|--------|
| | | | Simulation | Simulation | | Simulation | Simulation | |
| 20 | 14.77 | 92.34 | 0.1807 | 99.45 | 3.73 | | | 126.90 |
| 30 | 18.75 | 81.6 | 0.1525 | 141.60 | 3.72 | | | 205.30 |
| 40 | 18.93 | 69.27 | 0.1285 | 203.80 | 6.652 | | | 263.80 |
| 50 | 17.94 | 62.79 | 0.1175 | 280.40 | 9.32 | | | 304.70 |
| 60 | 16.43 | 58.76 | 0.1079 | 375.30 | 12.08 | | | 347.10 |
| 70 | 14.42 | 53.62 | 0.1016 | 451.50 | 14.62 | | | 373.90 |
| 80 | 15.58 | 50.16 | 0.0891 | 602.80 | 18.02 | | | 411.10 |
| 90 | 13.23 | 46.61 | 0.0851 | 702.80 | 24.11 | | | 434.80 |
| 100 | 17.12 | 42.32 | 0.0750 | 769.40 | 36.34 | | | 453.70 |

Table 14
Experimental validation.

| Load = 50% and Hydrogen premixing = 18% | | | | | | | | |
|---|---------------------------|-------|-------|------|-------|-----------------|---------------|------|
| Results | Peak in-cylinder pressure | BTE | BSEC | HC | CO | NO _x | Smoke opacity | EGT |
| RSM Optimized | 61.016 | 28.18 | 14.8 | 64 | 0.12 | 280 | 9.184 | 300 |
| ANN predicted | 61.04 | 27.37 | 14.81 | 62.8 | 0.118 | 280 | 9.32 | 305 |
| Experimented | 62.82 | 27.82 | 15.02 | 65 | 0.123 | 295 | 9.8 | 319 |
| RSM Relative error | 0.04 | | 1.29 | 1.46 | 1.54 | 2.44 | 5.08 | 5.96 |
| ANN Relative error | 2.83 | | 1.62 | 1.40 | 3.40 | 4.47 | 4.95 | 4.48 |

- The implemented RSM tool optimizes the experiments and gives the regression model for peak in-cylinder pressure, BE, BSEC, HC, CO, NO_x, smoke opacity, and EGT with responses of more than 95% desirability. This shows that the models that have been made can show how the induction of hydrogen affects the 40% ammonia biodiesel combustion on CI engine behavior.
- The RSM-based optimization research recommends 14.77%, 18.75%, 18.93%, 17.94%, 16.43%, 14.42%, 15.58%, 13.23% and 17.12% hydrogen proportion for 20%, 30%, 40%, 50%, 60%, 70%, 80%, 90% and 100% to increase performance and lower emission characteristics.
- RSM optimization with a desirability level of 97.9% was conducted over three trials for authentication using ANN. Based on the results, ANN predicts all the replies with R > 0.96, which shows a real-time replica of engine responses compared to the RSM model.

From the results of study, hydrogen could be used as an additive in the ammonia biofuel combustion process. Since the way an engine works depends on a lot of working factors, it's important to do more study on this kind of method to find out what works best.

Author statement

The authors would like to thank the reviewer for their time and valuable comments. We have modified the manuscript based on the reviewer's suggestion, and the detailed corrections are listed below point by point for the reviewer's perusal. To address the reviewer's comments and improve the quality of the manuscript 2 tables are updated, introduction and results section. To enhance the introduction and results section, 22 recent papers were included to strengthen the discussions and improve the understanding. Kindly consider our responses and consider for publication.

Declaration of competing interest

The authors declare that they have no known competing financial interests or personal relationships that could have appeared to

influence the work reported in this paper.

Data availability

Data will be made available on request.

Acknowledgement

The authors desire to show gratitude to the School of Mechanical Engineering, Vellore Institute of Technology (VIT), Vellore for the economic support extended in carrying out this research work.

Abbreviations

| | |
|------|--|
| RCCI | Reactivity controlled compression ignition |
| ANN | Artificial Neural Network |
| RSM | Response Surface Methodology |
| LRF | Low Reactive Fuel |
| HRF | High Reactive Fuel |
| BTE | brake specific fuel consumption |
| BSEC | brake specific energy consumption |

References

- [1] Y. Niki, Y. Nitta, H. Sekiguchi, K. Hirata, Diesel fuel multiple injection effects on emission characteristics of diesel engine mixed ammonia gas into intake air, *J. Eng. Gas Turbines Power* 141 (2019), <https://doi.org/10.1115/1.4042507>.
- [2] D. Scott, S. Becken, Adapting to climate change and climate policy: progress, Problems and potentials, *J. Sustain. Tourism* 18 (2010) 283–295, <https://doi.org/10.1080/09669581003668540>.
- [3] S. Yu, S. Zheng, X. Li, The achievement of the carbon emissions peak in China: the role of energy consumption structure optimization, *Energy Econ.* 74 (2018) 693–707, <https://doi.org/10.1016/j.eneco.2018.07.017>.
- [4] S. Simsek, H. Saygin, B. Ozdalyan, Improvement of fuel oil features and effect of its use in different compression ratios for an SI engine on performance and emission, *Energies* 13 (2020), <https://doi.org/10.3390/en13071824>.
- [5] J.S. Cardoso, V. Silva, R.C. Rocha, M.J. Hall, M. Costa, D. Eusébio, Ammonia as an energy vector: current and future prospects for low-carbon fuel applications in internal combustion engines, *J. Clean. Prod.* (2021) 296, <https://doi.org/10.1016/j.jclepro.2021.126562>.
- [6] Y. Guo, Z. Pan, L. An, Carbon-free sustainable energy technology: direct ammonia fuel cells, *J. Power Sources* 476 (2020), 228454, <https://doi.org/10.1016/j.jpowsour.2020.228454>.
- [7] B. Johnston, M.C. Mayo, A. Khare, Hydrogen: the energy source for the 21st century, *Technovation* 25 (2005) 569–585, <https://doi.org/10.1016/j.technovation.2003.11.005>.
- [8] Z. Said, D.T.N. Le, P. Sharma, V.H. Dang, H.S. Le, D.T. Nguyen, et al., Optimization of combustion, performance, and emission characteristics of a dual-fuel diesel engine powered with microalgae-based biodiesel/diesel blends and oxyhydrogen, *Fuel* 326 (2022), 124987, <https://doi.org/10.1016/j.fuel.2022.124987>.
- [9] A.T. Hoang, Experimental study on spray and emission characteristics of a diesel engine fueled with preheated bio-oils and diesel fuel, *Energy* 171 (2019) 795–808, <https://doi.org/10.1016/j.energy.2019.01.076>.
- [10] Simsek S, Uslu S, Simsek H. Comparison of the changes in diesel engine characteristics caused by the addition of 2-EHN cetane improver according to the use of diesel and second-generation biodiesel. <https://doi.org/10.1080/10916466.2022.2113097>.
- [11] S. SIMSEK, Increasing cetane number of the petrochemical machines by different fuel additives, *Int. J. Automot. Sci. Technol.* (2020), <https://doi.org/10.30939/ijastech..795984>.
- [12] E. Ansari, M. Shahbakti, J. Naber, Optimization of performance and operational cost for a dual mode diesel-natural gas RCCI and diesel combustion engine, *Appl. Energy* 231 (2018) 549–561, <https://doi.org/10.1016/j.apenergy.2018.09.040>.
- [13] A.T. Hoang, A.T. Le, Trilateral correlation of spray characteristics, combustion parameters, and deposit formation in the injector hole of a diesel engine running on preheated Jatropha oil and fossil diesel fuel, *Biofuel.Res.* J. 6 (2019) 909–919, <https://doi.org/10.18331/BRJ2019.6.1.2>.
- [14] P. Sharma, Artificial intelligence-based model prediction of biodiesel-fueled engine performance and emission characteristics: a comparative evaluation of gene expression programming and artificial neural network, *Heat Transfer* 50 (2021) 5563–5587, <https://doi.org/10.1002/htj.22138>.
- [15] H.C. Ong, Y.W. Tiong, B.H.H. Goh, Y.Y. Gan, M. Mofijur, I.M.R. Fattah, et al., Recent advances in biodiesel production from agricultural products and microalgae using ionic liquids: opportunities and challenges, *Energy Convers. Manag.* 228 (2021), 113647, <https://doi.org/10.1016/j.enconman.2020.113647>.
- [16] K. Brindhadevi, T. Mathimani, E.R. Rene, S. Shanmugam, N.T.L. Chi, A. Pugazhendhi, Impact of cultivation conditions on the biomass and lipid in microalgae with an emphasis on biodiesel, *Fuel* 284 (2021), 119058, <https://doi.org/10.1016/j.fuel.2020.119058>.
- [17] A.T. Hoang, M. Tabatabaei, M. Aghbashlo, A.P. Carlucci, A.I. Ölcer, A.T. Le, et al., Rice bran oil-based biodiesel as a promising renewable fuel alternative to petrodiesel: a review, *Renew. Sustain. Energy Rev.* 135 (2021), <https://doi.org/10.1016/j.rser.2020.110204>.
- [18] S. Simsek, S. Uslu, H. Simsek, Evaluation of the effect of a new alternative fuel containing boron and hydrogen on gasoline engine performance and emission responses, *Int. J. Environ. Sci. Technol.* 19 (2022) 4913–4922, <https://doi.org/10.1007/s13762-021-03460-6>.
- [19] A.T. Hoang, T Le Anh, A. Rahman, M. Al, V.V. Le, Measurement and prediction of the density and viscosity of biodiesel blends. <https://doi.org/10.14716/ijtech.v9i5.1950>, 2018.
- [20] A.E. Atabani, A.S. Silitonga, I. Anjum, T.M.I. Mahlia, H.H. Masjuki, S. Mekhilef, A comprehensive review on biodiesel as an alternative energy resource and its characteristics, *Renew. Sustain. Energy Rev.* 16 (2012) 2070–2093, <https://doi.org/10.1016/j.rser.2012.01.003>.
- [21] A.J. Kings, R.E. Raj, L.R.M. Miriam, M.A. Visvanathan, Cultivation, extraction and optimization of biodiesel production from potential microalgae Euglena sanguinea using eco-friendly natural catalyst, *Energy Convers. Manag.* 141 (2017) 224–235, <https://doi.org/10.1016/j.enconman.2016.08.018>.
- [22] A. Devaraj, Y. Devarajan, I. Vinoth Kannan, Investigation on emission pattern of biodiesel and Nano-particles, *Int. J. Ambient Energy* 42 (2021) 1103–1107, <https://doi.org/10.1080/01430750.2019.1586765>.
- [23] A.N. Ozsezen, M. Canakci, A. Turkcan, C. Sayin, Performance and combustion characteristics of a DI diesel engine fueled with waste palm oil and canola oil methyl esters, *Fuel* 88 (2009) 629–636, <https://doi.org/10.1016/j.fuel.2008.09.023>.

- [24] O.D. Samuel, M. Kaveh, O.J. Oyejide, P.V. Elumalai, T.N. Verma, K.S. Nisar, et al., Performance comparison of empirical model and Particle Swarm Optimization & its boiling point prediction models for waste sunflower oil biodiesel, *Case Stud. Therm. Eng.* 33 (2022), 101947, <https://doi.org/10.1016/j.csite.2022.101947>.
- [25] P. Rosha, A. Dhir, S. Kumar, Influence of gaseous fuel induction on the various engine characteristics of a dual fuel compression ignition engine : a review, *Renew. Sustain. Energy Rev.* (2017), <https://doi.org/10.1016/j.rser.2017.10.055>, 0–1.
- [26] S.P. Wategave, N.R. Banapurmath, M.S. Sawant, M.E.M. Soudagar, M.A. Mujtaba, A. Afzal, et al., Clean combustion and emissions strategy using reactivity controlled compression ignition (RCCI) mode engine powered with CNG-Karanja biodiesel, *J. Taiwan Inst. Chem. Eng.* 124 (2021) 116–131, <https://doi.org/10.1016/j.jtice.2021.04.055>.
- [27] P.V. Elumalai, M. Parthasarathy, J.S.C.I.I.J.R. Lalvani, H. Mehbob, O.D. Samuel, C.C. Enweremadu, et al., Effect of injection timing in reducing the harmful pollutants emitted from CI engine using N-butanol antioxidant blended eco-friendly Mahua biodiesel, *Energy Rep.* 7 (2021) 6205–6221, <https://doi.org/10.1016/j.egyrep.2021.09.028>.
- [28] S. Yasir, A. Siddiki, M. Mofjuri, P.S. Kumar, S. Forruque, H. Chyuan, et al., Microalgae biomass as a sustainable source for biofuel , biochemical and biobased value-added products : an integrated biorefinery concept, *Fuel* 307 (2022), 121782, <https://doi.org/10.1016/j.fuel.2021.121782>.
- [29] S. Rajamohan, A. Hari, K. Raja, Z. Huang, Evaluation of oxidation stability and engine behaviors operated by *Prosopis juliflora* biodiesel /diesel fuel blends with presence of synthetic antioxidant, *Sustain. Energy Technol. Assessments* 52 (2022), 102086, <https://doi.org/10.1016/j.seta.2022.102086>.
- [30] A.T. Hoang, M. Tabatabaei, M. Aghbashlo, A review of the effect of biodiesel on the corrosion behavior of metals /alloys in diesel engines, *Energy Sources, Part A Recovery, Util. Environ. Eff.* 0 (2019) 1–21, <https://doi.org/10.1080/15567036.2019.1623346>.
- [31] S. Erdogan, M.K. Balki, C. Sayin, The effect on the knock intensity of high viscosity biodiesel use in a DI diesel engine, *Fuel* 253 (2019) 1162–1167, <https://doi.org/10.1016/j.fuel.2019.05.114>.
- [32] S. Simsek, S. Uslu, H. Simsek, Assessment of the fuel recovery potential of cattle, sheep, and chicken waste fats in diesel engine, *Int. J. Environ. Sci. Technol.* 19 (2022) 11409–11420, <https://doi.org/10.1007/S13762-021-03851-9-METRICS>.
- [33] P. Murugesan, A.T. Hoang, E. Perumal Venkatesan, D. Santosh Kumar, D. Balasubramanian, A.T. Le, et al., Role of hydrogen in improving performance and emission characteristics of homogeneous charge compression ignition engine fueled with graphite oxide nanoparticle-added microalgae biodiesel/diesel blends, *Int. J. Hydrogen Energy* (2021), <https://doi.org/10.1016/j.ijhydene.2021.08.107>.
- [34] M. Ester, Influence of Exhaust Gas Recirculation on Combustion and Emission Characteristics of Diesel Engine Fuelled with 100 % Waste Cooking Oil, vol. 0, *Waste Biomass Valorization*, 2018, p. 0, <https://doi.org/10.1007/s12649-018-0194-0>.
- [35] P. Boomadevi, *Impact of Microalgae Biofuel on Microporous Turbine Aviation Engine: A Combustion and Emission Study*, 2021, p. 7.
- [36] A.K. Azad, I.C. Dedioussi, M De Jonnion, R.X. Fernandes, P. Glarborg, H. Hashemi, et al., Review on ammonia as a potential fuel : from synthesis to economics, <https://doi.org/10.1021/acs.energyfuels.0c03685>, 2021.
- [37] A.J. Reiter, S.C. Kong, Demonstration of compression-ignition engine combustion using ammonia in reducing greenhouse gas emissions, *Energy Fuel.* 22 (2008) 2963–2971, <https://doi.org/10.1021/ef800140f>.
- [38] B. Zincir, Environmental and economic evaluation of ammonia as a fuel for short-sea shipping: a case study, *Int. J. Hydrogen Energy* 47 (2022) 18148–18168, <https://doi.org/10.1016/j.ijhydene.2022.03.281>.
- [39] A.J. Reiter, S.C. Kong, Diesel Engine Operation Using Ammonia as a Carbon-free Fuel, *American Society of Mechanical Engineers, Internal Combustion Engine Division (Publication) ICE*, 2010, pp. 111–117, <https://doi.org/10.1115/ICEF2010-35026>.
- [40] T. Saika, M. Nakamura, T. Nohara, S. Ishimatsu, Study of hydrogen supply system with ammonia fuel, *JSME Int. J. Ser. B Fluids Therm. Eng.* 49 (2006) 78–83, <https://doi.org/10.1299/jstmeb.49.78>.
- [41] W.L. Ahlgren, The dual-fuel strategy: an energy transition plan, *Proc. IEEE* 100 (2012) 3001–3052, <https://doi.org/10.1109/JPROC.2012.2192469>.
- [42] J. Frost, A. Tall, A.M. Sheriff, A. Schönborn, P. Hellier, An experimental and modelling study of dual fuel aqueous ammonia and diesel combustion in a single cylinder compression ignition engine, *Int. J. Hydrogen Energy* 46 (2021) 35495–35510, <https://doi.org/10.1016/j.ijhydene.2021.08.089>.
- [43] S. Oh, C. Park, J. Oh, S. Kim, Y. Kim, Y. Choi, et al., Combustion, emissions, and performance of natural gas–ammonia dual-fuel spark-ignited engine at full-load condition, *Energy* 258 (2022), 124837, <https://doi.org/10.1016/j.energy.2022.124837>.
- [44] A. Yousefi, H. Guo, S. Dev, S. Lafrance, B. Liko, A study on split diesel injection on thermal efficiency and emissions of an ammonia/diesel dual-fuel engine, *Fuel* 316 (2022), 123412, <https://doi.org/10.1016/j.fuel.2022.123412>.
- [45] Z. Liu, L. Zhou, L. Zhong, H. Wei, Enhanced combustion of ammonia engine based on novel air-assisted pre-chamber turbulent jet ignition, *Energy Convers. Manag.* 276 (2023), 116526, <https://doi.org/10.1016/j.enconman.2022.116526>.
- [46] Y. Feng, J. Zhu, Y. Mao, M. Raza, Y. Qian, L. Yu, et al., Low-temperature auto-ignition characteristics of NH3/diesel binary fuel: ignition delay time measurement and kinetic analysis, *Fuel* 281 (2020), 118761, <https://doi.org/10.1016/j.fuel.2020.118761>.
- [47] A.M. Elbaz, S. Wang, T.F. Guibert, W.L. Roberts, Review on the recent advances on ammonia combustion from the fundamentals to the applications, *Fuel Communications* 10 (2022), 100053, <https://doi.org/10.1016/j.jfueco.2022.100053>.
- [48] T. Vinoth, P. Vasanthakumar, J. Krishnaraj, S.K. Arunsankar, J. Hariharan, M. Palanisamy, Experimental investigation on LPG + diesel fuelled engine with DEE ignition improver, *Mater Today Proc.* 4 (2017) 9126–9132, <https://doi.org/10.1016/j.matpr.2017.07.268>.
- [49] A. Yousefi, H. Guo, M. Birouk, Effect of diesel injection timing on the combustion of natural gas/diesel dual-fuel engine at low-high load and low-high speed conditions, *Fuel* 235 (2019) 838–846, <https://doi.org/10.1016/j.fuel.2018.08.064>.
- [50] K. Panda, A. Ramesh, Parametric investigations to establish the potential of methanol based RCCI engine and comparison with the conventional dual fuel mode, *Fuel* 308 (2022), 122025, <https://doi.org/10.1016/j.fuel.2021.122025>.
- [51] A. Yousefi, H. Guo, S. Dev, B. Liko, S. Lafrance, Effects of ammonia energy fraction and diesel injection timing on combustion and emissions of an ammonia/diesel dual-fuel engine, *Fuel* 314 (2022), 122723, <https://doi.org/10.1016/j.fuel.2021.122723>.
- [52] B.A. Oni, S.E. Sanni, A.J. Ibegbu, T.E. Amoo, Investigating the emissions and performance of hydrogen enriched-biogas-Parinari polyandra biodiesel in a direct injection (DI) engine, *Int. J. Hydrogen Energy* 47 (2022) 29945–29955, <https://doi.org/10.1016/j.ijhydene.2022.06.292>.
- [53] M.H. Dinesh, Study of performance, combustion and NO emission behavior of an S engine fuelled with ammonia/hydrogen blends at various compression ratio, Pandey JK, Kumar GN, Study of performance, combustion, and NOx emission behavior of an SI engine fuelled with ammonia/hydrogen blends at various compression ratio, *Int. J. Hydrogen Energy* 47 (2022) 25391–25403, <https://doi.org/10.1016/j.ijhydene.2022.05.287>.
- [54] G.K. Lilik, H. Zhang, J.M. Herreros, D.C. Haworth, A.L. Boehman, Hydrogen assisted diesel combustion, *Int. J. Hydrogen Energy* 35 (2010) 4382–4398, <https://doi.org/10.1016/j.ijhydene.2010.01.105>.
- [55] B. Wang, C. Yang, H. Wang, D. Hu, Y. Wang, Effect of Diesel-Ignited Ammonia/Hydrogen mixture fuel combustion on engine combustion and emission performance, *Fuel* 331 (2023), 125865, <https://doi.org/10.1016/j.fuel.2022.125865>.
- [56] W. Tutak, A. Jamrozik, K. Grab-Rogalski, Effect of natural gas enrichment with hydrogen on combustion process and emission characteristic of a dual fuel diesel engine, *Int. J. Hydrogen Energy* 45 (2020) 9088–9097, <https://doi.org/10.1016/j.ijhydene.2020.01.080>.
- [57] V. Praveena, Shobana Bai FJJ, D. Balasubramanian, Y. Devarajan, F. Aloui, E.G. Varuvel, Experimental assessment on the performance, emission and combustion characteristics of a safflower oil fueled CI engine with hydrogen gas enrichment, *Fuel* 334 (2023), 126682, <https://doi.org/10.1016/j.fuel.2022.126682>.
- [58] N. Seelam, S.K. Gugulothu, R.V. Reddy, B. Bhasker, J. Kumar Panda, Exploration of engine characteristics in a CRDI diesel engine enriched with hydrogen in dual fuel mode using toroidal combustion chamber, *Int. J. Hydrogen Energy* 47 (2022) 13157–13167, <https://doi.org/10.1016/j.ijhydene.2022.02.056>.
- [59] P. Dimitriou, R. Javaid, A review of ammonia as a compression ignition engine fuel, *Int. J. Hydrogen Energy* 45 (2020) 7098–7118, <https://doi.org/10.1016/j.ijhydene.2019.12.209>.
- [60] C. Liew, H. Li, J. Nuszkowski, S. Liu, T. Gatts, R. Atkinson, et al., An Experimental Investigation of the Combustion Process of a Heavy-Duty Diesel Engine Enriched with H₂, vol. 5, 2010, <https://doi.org/10.1016/j.ijhydene.2010.06.023>, 0–8.

- [61] H. Köse, M. Ciniviz, An experimental investigation of effect on diesel engine performance and exhaust emissions of addition at dual fuel mode of hydrogen, *Fuel Process. Technol.* 114 (2013) 26–34, <https://doi.org/10.1016/j.fuproc.2013.03.023>.
- [62] P. Saiteja, B. Ashok, Study on interactive effects of CRDi engine operating parameters through RSM based multi-objective optimization technique for biofuel application, *Energy* 255 (2022), 124499, <https://doi.org/10.1016/j.energy.2022.124499>.
- [63] M. Aydin, S. Uslu, M. Bahattin Çelik, Performance and emission prediction of a compression ignition engine fueled with biodiesel-diesel blends: a combined application of ANN and RSM based optimization, *Fuel* 269 (2020), <https://doi.org/10.1016/j.fuel.2020.117472>.
- [64] S. Dey, N.M. Reang, P.K. Das, M. Deb, Comparative study using RSM and ANN modelling for performance-emission prediction of CI engine fuelled with biodiesohol blends: fuzzy optimization approach, *Fuel* 292 (2021), 120356, <https://doi.org/10.1016/j.fuel.2021.120356>.
- [65] S. Sathyaranayanan, S. Suresh, S. Uslu, R.S. Shivarajani, V.P. Chandramohan, S. Simsek, Optimization of gasoline engine emission parameters employing commercial and sucrolite-catalyst coated converter using response surface methodology, *Int. J. Environ. Sci. Technol.* 20 (2023) 1725–1738, <https://doi.org/10.1007/S13762-022-03968-5/METRICS>.
- [66] S. Simsek, S. Uslu, H. Simsek, G. Uslu, Multi-objective-optimization of process parameters of diesel engine fueled with biodiesel/2-ethylhexyl nitrate by using Taguchi method, *Energy* 231 (2021), <https://doi.org/10.1016/j.energy.2021.120866>.
- [67] S. Simsek, S. Uslu, Investigation of the effects of biodiesel/2-ethylhexyl nitrate (EHN) fuel blends on diesel engine performance and emissions by response surface methodology (RSM), *Fuel* 275 (2020), <https://doi.org/10.1016/j.fuel.2020.118005>.
- [68] S. Simsek, S. Uslu, Experimental study of the performance and emissions characteristics of fusel oil/gasoline blends in spark ignited engine using response surface methodology, *Fuel* 277 (2020), <https://doi.org/10.1016/j.fuel.2020.118182>.
- [69] S. Simsek, S. Uslu, H. Simsek, G. Uslu, Improving the combustion process by determining the optimum percentage of liquefied petroleum gas (LPG) via response surface methodology (RSM) in a spark ignition (SI) engine running on gasoline-LPG blends, *Fuel Process. Technol.* (2021) 221, <https://doi.org/10.1016/j.fuproc.2021.106947>.
- [70] S. Simsek, S. Uslu, Determination of a diesel engine operating parameters powered with canola, safflower and waste vegetable oil based biodiesel combination using response surface methodology (RSM), *Fuel* 270 (2020), <https://doi.org/10.1016/j.fuel.2020.117496>.
- [71] S. Simsek, S. Uslu, H. Simsek, Response surface methodology-based parameter optimization of single-cylinder diesel engine fueled with graphene oxide dosed sesame oil/diesel fuel blend, *Energy and AI* 10 (2022), <https://doi.org/10.1016/j.egyai.2022.100200>.
- [72] S. Uslu, S. Simsek, H. Simsek, RSM modeling of different amounts of nano-TiO₂ supplementation to a diesel engine running with hemp seed oil biodiesel/diesel fuel blends, *Energy* 266 (2023), <https://doi.org/10.1016/j.energy.2022.126439>.
- [73] S. Simsek, S. Uslu, H. Simsek, Proportional impact prediction model of animal waste fat-derived biodiesel by ANN and RSM technique for diesel engine, *Energy* 239 (2022), <https://doi.org/10.1016/j.energy.2021.122389>.
- [74] T.F. Yusaf, B.F. Yusuf, M.M. Elawad, Crude palm oil fuel for diesel-engines: experimental and ANN simulation approaches, *Energy* 36 (2011) 4871–4878, <https://doi.org/10.1016/J.ENERGY.2011.05.032>.
- [75] E. Nadimi, G. Przybyla, M.T. Lewandowski, W. Adamczyk, Effects of ammonia on combustion, emissions, and performance of the ammonia/diesel dual-fuel compression ignition engine, *J. Energy Inst.* 107 (2023), <https://doi.org/10.1016/j.joei.2022.101158>.
- [76] S. Simsek, S. Uslu, H. Simsek, Experimental study on the ability of different biogas level dual fuel spark ignition engine: emission mitigation, performance, combustion . *Anal.* 76 (2021) 74, <https://doi.org/10.2516/ogst/2021060i>.
- [77] S. Simsek, B. Ozdalyan, Improvements to the composition of fusel oil and analysis of the effects of fusel oil-gasoline blends on a spark-ignited (SI) engine's performance and emissions, *Energies* 11 (2018), <https://doi.org/10.3390/en11030625>.
- [78] S. SIMSEK, S. Uslu, Analysis of the effects of cetane improver addition to diesel on engine performance and emissions, *Int. J. Adv. Eng. Technol.* (2021) 26–32, <https://doi.org/10.18245/ijaet.798221>.
- [79] S. Simsek, S. Uslu, R. Coştu, A novel approach to study the effect of motor silk-added pyrolysis tire oil on performance and emission characteristics of a diesel engine, *Fuel* 288 (2021), <https://doi.org/10.1016/j.fuel.2020.119668>.
- [80] S. Simsek, S. Uslu, M. Sahin, F. Arlı, G. Bilgic, Impact of a novel fuel additive containing boron and hydrogen on diesel engine performance and emissions, *Energy Sources, Part A Recovery, Util. Environ. Eff.* (2021), <https://doi.org/10.1080/15567036.2021.1946621>.
- [81] S. Simsek, Effects of biodiesel obtained from Canola, safflower oils and waste oils on the engine performance and exhaust emissions, *Fuel* 265 (2020), <https://doi.org/10.1016/j.fuel.2020.117026>.
- [82] A.M. Elbaz, S. Wang, T.F. Guiberti, W.L. Roberts, Review on the recent advances on ammonia combustion from the fundamentals to the applications, *Fuel Communications* 10 (2022), 100053, <https://doi.org/10.1016/j.jfueco.2022.100053>.
- [83] S. Simsek, S. Uslu, Comparative evaluation of the influence of waste vegetable oil and waste animal oil-based biodiesel on diesel engine performance and emissions, *Fuel* 280 (2020), <https://doi.org/10.1016/j.fuel.2020.118613>.
- [84] S. Simsek, S. Uslu, Investigation of the impacts of gasoline, biogas and LPG fuels on engine performance and exhaust emissions in different throttle positions on SI engine, *Fuel* 279 (2020), <https://doi.org/10.1016/j.fuel.2020.118528>.